AD-A182 154 INVESTIGATION OF THE ELASTIC BEHAVIOR OF AL-LI-X ALLOYS 1/2
(U) VIRGINIA UNIV CHARLOTTESVILLE DEPT OF MATERIALS
SCIENCE W W RUCH ET AL 01 JUN 87 UVA/525400/MS87/102
UNCLASSIFIED N00014-85-K-0526 F/G 11/6 1 NL

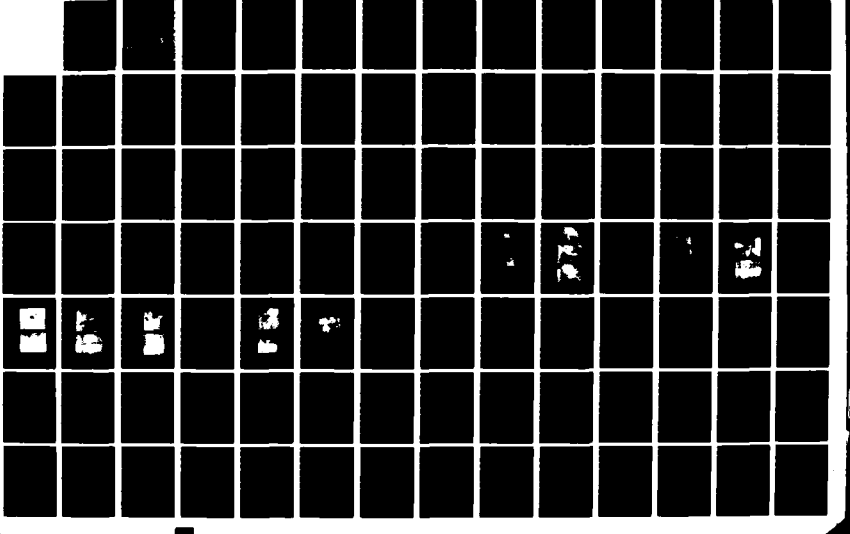

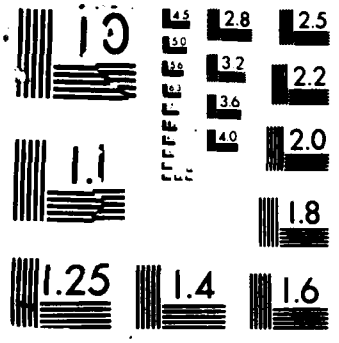
1.0
1.1
1.25
1.4
1.6
1.8
2.0
2.2
2.5
2.8
3.2
3.6
4.0
4.5
5.0
5.6

(12

A Final Report
Grant No. N00014-85-K-0526
June 1, 1985 - May 31, 1987

INVESTIGATION OF THE ELASTIC BEHAVIOR OF AL-Li-X ALLOYS

Submitted to:

Office of Naval Research
800 North Quincy Street
Arlington, VA 22217-5000

Attention: Dr. Bruce A. MacDonald, Manager
Metallic Materials Program
Code 1131M

Submitted by:

W. W. Ruch
Research Assistant Professor

E. A. Starke, Jr.
Professor and Dean

Report No. UVA/525400/MS87/102
June 1987

SCHOOL OF ENGINEERING AND
APPLIED SCIENCE

DEPARTMENT OF MATERIALS SCIENCE

UNIVERSITY OF VIRGINIA
CHARLOTTESVILLE, VIRGINIA 22901

A Final Report
Grant No. N00014-85-K-0526
June 1, 1985 - May 31, 1987

INVESTIGATION OF THE ELASTIC BEHAVIOR OF AL-Li-X ALLOYS

Submitted to:

Office of Naval Research
800 North Quincy Street
Arlington, VA 22217-5000

Attention: Dr. Bruce A. MacDonald, Manager
Metallic Materials Program
Code 1131M

Submitted by:

W. W. Ruch
Research Assistant Professor

E. A. Starke, Jr.
Professor and Dean

Department of Materials Science
SCHOOL OF ENGINEERING AND APPLIED SCIENCE
UNIVERSITY OF VIRGINIA
CHARLOTTESVILLE, VIRGINIA

Report No. UVA/525400/MS87/102

Copy No. 13

June 1987

unclassified

SECURITY CLASSIFICATION OF THIS PAGE

REPORT DOCUMENTATION PAGE

1a. REPORT SECURITY CLASSIFICATION Unclassified	1b. RESTRICTIVE MARKINGS None
2a. SECURITY CLASSIFICATION AUTHORITY	3. DISTRIBUTION/AVAILABILITY OF REPORT Approved for Public Release; Distribution Unlimited
2b. DECLASSIFICATION/DOWNGRADING SCHEDULE	
4. PERFORMING ORGANIZATION REPORT NUMBER(S) UVA/525400/MS87/102	5. MONITORING ORGANIZATION REPORT NUMBER(S)
6a. NAME OF PERFORMING ORGANIZATION Dept. of Materials Science University of Virginia 6b. OFFICE SYMBOL (If applicable)	7a. NAME OF MONITORING ORGANIZATION Office of Naval Research Resident Representative
6c. ADDRESS (City, State, and ZIP Code) Thornton Hall Charlottesville, VA 22901	7b. ADDRESS (City, State, and ZIP Code) Joseph Henry Building, Room 623 2100 Pennsylvania Avenue, N.W. Washington, D.C. 20037
8a. NAME OF FUNDING/SPONSORING ORGANIZATION Dept. of Navy Office of Naval Research 8b. OFFICE SYMBOL (If applicable) N00014	9. PROCUREMENT INSTRUMENT IDENTIFICATION NUMBER N00014-85-K-0526
8c. ADDRESS (City, State, and ZIP Code) 800 North Quincy Street Arlington, VA 22217-5000	10. SOURCE OF FUNDING NUMBERS PROGRAM ELEMENT NO. / PROJECT NO. / TASK NO. / WORK UNIT ACCESSION NO.

11. TITLE (Include Security Classification)

Investigation of the Elastic Behavior of Al-Li-X Alloys

12 PERSONAL AUTHOR(S)

W. W. Ruch, E. A. Starke, Jr.

13a. TYPE OF REPORT	13b. TIME COVERED	14. DATE OF REPORT (Year, Month, Day)	15. PAGE COUNT
Final	FROM 6/1/85 TO 5/31/87	June 1, 1987	

16. SUPPLEMENTARY NOTATION

17. COSATI CODES			18. SUBJECT TERMS (Continue on reverse if necessary and identify by block number)
FIELD	GROUP	SUB-GROUP	

19 ABSTRACT (Continue on reverse if necessary and identify by block number)

Several Al(-Cu)(-Mg)-Li(-Zr) alloys were investigated. The Young's modulus, shear modulus and Poisson's ratio were determined using an ultrasonic pulse echo technique. The elastic properties were measured as a function of aging time, aging temperature, amount of stretching and testing direction. An increase in Young's modulus due to delta prime and T1 precipitation has been measured and treated quantitatively including precipitation kinetics. A significant decrease of about 5% in the modulus of elasticity can be found in peak age conditions. This decrease can be attributed to precipitation of the T2 phase. The shear modulus behaves similar to Young's modulus while the Poisson's ratio remains unchanged. There is no significant orientation dependence of the elastic properties on testing direction despite the fact that a typical rolling texture was present.

20 DISTRIBUTION/AVAILABILITY OF ABSTRACT	21 ABSTRACT SECURITY CLASSIFICATION
☒ UNCLASSIFIED/UNLIMITED ☐ SAME AS RPT ☐ DTIC USERS	Unclassified
22a NAME OF RESPONSIBLE INDIVIDUAL Dr. Bruce A. MacDonald	22b TELEPHONE (Include Area Code) (202) 696-4401
	22c. OFFICE SYMBOL N00014

DD FORM 1473, 84 MAR 83 APR edition may be used until exhausted. All other editions are obsolete.

SECURITY CLASSIFICATION OF THIS PAGE

unclassified

TABLE OF CONTENTS

LIST OF FIGURES

LIST OF TABLES

LIST OF SYMBOLS

SYMBOL	DESCRIPTION
amu	Atomic Mass Units
CWQ	Cold Water Quench
D	Density
E	Young's Modulus
e	Strain
EDAX	Energy Dispersive X-ray Analysis
EDS	Energy Dispersive Spectroscopy
EELS	Electron Energy Loss Spectroscopy
G	Shear Modulus
GP zones	Guinier-Preston zones (a precipitate phase)
LT	Long Transverse direction
Q	Precipitate phase (composition undetermined)
R	Precipitate Phase (Al_5CuLi_3)
S	Stress
s	Poisson's Ratio
SAXS	Small Angle X-ray Scattering
ST	Short Transverse direction
SEM	Scanning Electron Microscope
SHT	Solution Heat Treated
SSSS	Super saturated solid solution
T1	Precipitate Phase (Al_2CuLi)
T2	Precipitate Phase (Al_6CuLi_3)
TB	Precipitate Phase ($Al_{7.5}Cu_4Li$)

TEM	Transmission Electron Microscope
δ'	Precipitate Phase (Al_3Li)
δ	Precipitate Phase (AlLi)
θ	Precipitate Phase (Al_2Cu)

CHAPTER 1

INTRODUCTION

The objective of this study is to examine the important parameters influencing the elastic modulus in commercially important aluminum-lithium alloys as a function of microstructure. These parameters include type of phases, measurement of volume fractions, examination of the interaction between the phases, and orientation effects. The results can be used to produce aluminum-lithium alloys with an optimized elastic modulus.

It is well established that the addition of lithium to aluminum decreases the density and increases the elastic modulus (1,2,3,4). Aluminum-lithium alloys offer lower density, and higher stiffness than any aluminum alloy. These properties are important for aerospace applications. The aluminum-lithium alloys are a potential substitute for the currently used 2000 and 7000 series aluminum alloys used in aircraft (5). Implementation of aluminum-lithium alloys will result in structural weight reductions up to 15% (6) and therefore, significant cost savings. These savings are the impetus for the extensive amount of research that has taken place in aluminum-lithium alloy research since the 1970's (7).

The decrease in density which occurs when lithium is added to aluminum is well understood (2). Lithium has a lower atomic weight than aluminum. The atomic weight of lithium is approximately one fourth that of aluminum. Also, when lithium is added to aluminum, the lattice parameter of the solid solution remains essentially constant (8). These two factors are the reasons for the lower density.

The increase in modulus with the addition of lithium is not as well understood. The elastic modulus of lithium is more than six times smaller than that of aluminum. The reason why lithium causes an increase in the modulus when added to aluminum may be due to electronic effects (9,10).

Chapter 2

BACKGROUND

2.1 Elasticity

The fundamental law which governs elastic behavior is Hooke's law. This law states that in an elastic solid the strain is directly proportional to the applied stress. This is represented by the following equation (11):

$$S = E*e \qquad \text{eq. 2.1}$$

S - applied stress
E - proportionality constant (elastic modulus)
e - strain

Stress is a second rank tensor, specified by nine components. Strain is also a second rank tensor, represented by nine components. The elastic modulus, E, reflects the atomic binding forces of the material. It is related to the electronic structure of the atoms. The modulus is represented by a fourth rank tensor comprised of elastic stiffness constants.

In a crystalline material, symmetry, which arises from the type of crystal structure, reduces the number of elastic constants. The required number of elastic constants necessary to characterize the elastic behavior of a cubic material, such as aluminum, is three (See figure 1) (12).

Elastic waves can be propagated through a single crystal cubic material in the [110] direction to determine the three elastic constants C_{11}, C_{12}, and C_{44}.

	e_{xx}	e_{yy}	e_{zz}	e_{yz}	e_{zx}	e_{xy}
X_x	C_{11}	C_{12}	C_{12}	0	0	0
Y_y	C_{12}	C_{11}	C_{12}	0	0	0
Z_z	C_{12}	C_{12}	C_{11}	0	0	0
Y_z	0	0	0	C_{44}	0	0
Z_x	0	0	0	0	C_{44}	0
X_y	0	0	0	0	0	C_{44}

Figure 1. The required number of elastic constants necessary to characterize the elastic behavior of a cubic material (12).

There are two shear waves and a transverse wave. In [110] directions the difference between velocities is greatest. Therefore, the shear waves are most easily resolved in this direction (13).

The elastic constants have been determined for a variety of cubic crystals (12). Several factors affect the elastic constants and hence, the elastic moduli. The elastic properties may vary with changes in temperature and pressure (14,15). They also change with alloying additions. The modulus of elasticity decreases with an increase in temperature. This is because the modulus varies inversely with the distance of atom or ion separation raised to the fourth power (11). Since the equilibrium distance of atom separation increases with an increase in temperature, the modulus will decrease with an increase in temperature. The modulus will be affected similarly by an increase in pressure or alloying additions. A change in the interatomic bonds dictates how the elastic modulus is altered.

2.1.1 Aluminum and Aluminum Solid Solutions

The elastic behavior of aluminum and aluminum alloy solid solutions is dependent upon the chemical composition and the electronic structure. Most alloying additions do not have a large effect on the electronic structure. However, lithium and magnesium are exceptions and they change the electronic structure significantly (76).

The (FCC) metal aluminum displays only a small degree of

anisotropy in comparison to other FCC metals, especially those with an electron valency of unity. Theoretical work done by Leigh in 1951 (9) concluded that the overlapping of the Fermi surfaces with the surfaces of the first Brillouin-zone and the virtual absence of non-Coulomb interactions play an important role in the elastic behavior of aluminum. Leigh explored in detail the possibility that the observed isotropy of aluminum may be the result of near compensation between the effects of the Coulomb energy term and the Fermi energy term. According to Leigh these two energy terms contribute to the bonding in aluminum. The Coulomb term arises from the energy between the positive atoms and the negative electron gas. The Fermi term is due to the overlapping electrons. It has been shown by Jones (16) that the contribution from non-Coulomb interactions to the elastic constants is negligible due to the large distance between ion cores.

Most dilute solid solutions of aluminum alloys display elastic behavior which is dependent upon the individual contributions form the metals present. A linear rule of mixtures is applicable. The modulus can be calculated from the individual contributions of the metals present, on a volume basis. Lithium and magnesium additions are exceptions. Lithium has a different valence electron concentration per atom than aluminum, and an appreciable amount of lithium can be put into solid solution with

aluminum. The elastic constants in aluminum solid solutions depend on the electron concentration. Leigh's theory calculates the elastic anisotropy as a function of the valence electron concentration (VEC) per atom in single phase aluminum alloys. Leigh predicts how the elastic constants of aluminum will change with additions of metals of higher or lower valency in solution. Leigh predicts that when metals of valency higher or lower than three dissolve substitutionally in aluminum there is a change in the number of free electrons. This consequently leads to a change in the contributions to the elastic constants from overlapping electron energies. Lithium additions fall into this category.

The primary effect that lithium has on the modulus of aluminum occurs when lithium is present in the solid solution. When lithium is added to aluminum there is virtually no change in the lattice parameter for the solid solution (8). Every element, when added to aluminum, changes the electronic structure of the alloy. The addition of lithium changes the electronic structure favorably in regard to the elastic modulus. Aluminum has a valence electron concentration of +3; lithium has a valence electron concentration of +1. Therefore, the addition of lithium decreases the number of free electrons. A decrease in the number of free electrons changes the elastic constants because of a change in the number of occupied states in the band scheme. This electronic effect may be the reason that lithium increases the elastic modulus so drastically when it

is present in solid solution with aluminum.

Muller et al. (17) have determined the elastic constants for several binary aluminum-lithium alloys in solid solution. In each case all three elastic constants increased with increasing lithium content. The higher elastic constants correspond to a higher Young's modulus and shear modulus.

2.1.2 Multiphase Alloys

The modulus of the alloy is composed of individual contributions from the various phases present. In precipitation hardenable aluminum-lithium alloys the largest phase is the matrix. The other phases present are constituent particles, dispersoids and strengthening precipitates. To have a significant effect on the elastic modulus these phases must have a modulus significantly different from the matrix or be present in significantly large volume fractions. Also, there may be a unique orientation effect for each phase.

Another important factor is the interaction between the matrix phase and the second phases present. How the stress and strain is transferred between the matrix and precipitate phases is dependent upon the characteristics of the interface between the various phases. The type of interface dictates if there is a total transfer of stress or strain or only a partial transfer. This interaction will influence the overall modulus.

Several models have been used to calculate the overall modulus of a multiphase material. These methods assume different types of interactions between the various phases.

Voigt averaging (18) assumes the elastic strain between the matrix and individual phases is uniform throughout the material. This is represented by the following equation:

$$E^m = \sum f_i * (E_i)^m \qquad \text{eq. 2.2}$$

E - modulus of the alloy
f_i - volume fraction of phase i
E_i - modulus of phase i

The Voigt model, (m=1), gives an upper limit. This method is a linear rule of mixtures.

Reuss averaging (19) assumes equal stress between the phases (m=-1). This is a lower limit. These two methods give the extreme values. Materials may exhibit a situation which is intermediate between these two extremes. Hill (20) proposed an arithmetic average of the two situations:

$$E_H = 1/2\ (E_V + E_R) \qquad \text{eq. 2.3}$$

M.E. Fine has shown that Voigt averaging fits the data of Al-$MnAl_6$ alloys where the modulus changes linearly with the volume fraction of $MnAl_6$ (21). Lyle reports data for Al-Al_2O_3 which fits the Reuss model better (22). Fine theorizes that the stress and strain may not be completely transferred in the Al-Al_2O_3 system due to poor bonding

between the phases (21). The type of averaging method is determined by the interactions of the various phases present.

In this investigation additions of lithium, copper and zirconium were alloyed with aluminum. The various alloying additions promote different phases.

Several important investigations have been performed on the addition of lithium (10,17,21,23). In aluminum-lithium alloys a primary second phase is the delta prime phase (Al_3Li). Muller et al. have determined the elastic constants of two phase aluminum-lithium alloys using the pulse echo technique (17). Several binary alloys with lithium contents up to 9.6 at% were examined as single crystals. The constants measured included a contribution from the matrix phase and the delta prime phase. The longitudinal mode gave the constant C_l. The transverse mode [001] gave the constant C and transverse mode [110] gave the constant C'. These constants represent the following (9):

$$Cl = (C_{11}+C_{12}+C_{44})/2 \qquad \text{eq. 2.4}$$

$$C' = (C_{11}-C_{12})/2 \qquad \text{eq. 2.5}$$

$$C = C_{44} \qquad \text{eq. 2.6}$$

The contribution from the matrix phase was determined from the limit of the miscibility gap given by Cocco et al. (24). The contribution from the precipitate phase was determined from a volume fraction of delta prime established from SAXS examination and using a rule of mixtures which takes an arithmetic average of the Voigt and Reuss averaging

techniques. Once the constants for the delta prime phase were calculated, the elastic modulus (E) was determined from the following relationships (75):

$$K = C_1 - C - C'/3 \qquad \text{eq. 2.7}$$

$$G = (2C+2C')/5 \qquad \text{eq. 2.8}$$

$$E = 9KG/(3K+G) \qquad \text{eq. 2.9}$$

The elastic modulus of delta prime was estimated to be 106 GPa.

These data also support the increase in elastic constants with increasing lithium in solid solution. The data showed that increasing the volume fraction of delta prime increased all three elastic constants. The coarsening of delta prime leads to a small increase in the constants Cl and C' and a decrease in C.

The elastic moduli of several binary polycrystalline aluminum-lithium alloys were investigated by B. Noble, S.J. Harris and K. Dinsdale (10). They examined additions of magnesium and lithium to aluminum. Static modulus determination techniques were used. They clearly demonstrated that the addition of lithium to aluminum increases the elastic modulus and that the addition of magnesium slightly decreases the elastic modulus.

They calculated the intrinsic modulus of the delta prime phase to be 96 GPa. They considered that the matrix was a solid solution phase. The amount of lithium in the matrix phase and the volume fraction of delta prime was determined from the delta prime solvus line. They assumed the amount

of lithium in the matrix phase to remain constant at 5.5 at%. Ceresara et al. (69) report the metastable solvus line at 6.1 at% for 170 C, the aging temperature used by Noble et al. The overall moduli were values in the range of 79 to 83 GPa.

M.S. Fine calculated the modulus of Al_3Li. The reported values were high, 140 GPa (21). Fine regarded the modulus of the matrix phase to be the same as pure aluminum. The matrix is a solid solution of aluminum-lithium; therefore, it has a higher modulus. The higher modulus of the matrix phase would cause an increase in the overall modulus of the alloy. Fine overestimated the contribution from the delta prime phase. Using Fine's data and correcting for the modulus of the matrix phase gives a modulus of 103.2 GPa for the delta prime phase. This value is close to the value obtained by Muller et al. (17). Noble et al. (10) calculated the modulus of the delta phase to be 105 GPa. The elastic modulus was not calculated for other phases containing lithium in any of these investigations.

Broussaud performed modulus measurements on binary aluminum-lithium alloys (23). An ultrasonic pulse echo technique was used. The results indicate a significant difference between the as-quenched alloys and the aged alloys. This difference is attributed to the precipitation of the delta prime phase. In these binary alloys there is no significant change in elastic modulus beyond several hours aging time.

The addition of copper to aluminum causes the precipitation of several different phases. For aluminum-copper alloys the elastic modulus at room temperature is of the order of 70 - 75 GPa (25). Experimental results by Fouquet et al. (26) show that θ precipitation causes an increase in the Young's modulus of up to 3%. The increase in modulus depends upon the precipitate size and the coherency state of the precipitate-matrix interface.

Agyekum et al. investigated the elastic modulus of several ternary Al-Cu-Li and quaternary Al-Cu-Li-Mg alloys (27). Their results indicate that the T1 phase (Al_2CuLi) contributes positively to the overall modulus. They also concluded that exceeding the solubility limit of lithium ties up the lithium in large equilibrium particles which have a negative effect on the Young's modulus. The ultrasonic pulse echo technique was used for these calculations.

Other phases may contribute positively or negatively to the elastic modulus. Both delta prime and T1 have a higher modulus value than the overall modulus. The volume fraction of precipitates present and the type of precipitates present will make a contribution to the total elastic modulus of the material.

The volume fraction of Al_3Zr in these alloys is small, typically between 0.1 and 0.2 volume percent. Therefore, the influence of the presence of these small amounts of

zirconium on the elastic modulus is negligible. Research done by Noble, Harris and Dinsdale (10) demonstrates that the presence of small amounts of zirconium has no effect on the modulus of aluminum-lithium binary alloys. If lithium is in the Al_3Zr dispersoids, there will not be a pronounced effect on the modulus due to the very small volume fraction.

2.1.3 Texture

The texture of a material describes the predominant crystallographic orientation of the crystals in a polycrystalline alloy. Each grain in a polycrystalline material has a different orientation. The texture of a material is a measurement of which orientations are most frequent. Many material properties such as strength, modulus, and formability are dependent on the texture (28).

In a single crystal material there is a difference in the modulus which is dependent upon crystallographic orientation. The maximum theoretical difference in modulus for a single crystal of aluminum is calculated to be approximately 20%. Theoretically, a polycrystalline material may approach the difference experienced in single crystals if it is highly textured. Usually, the difference measured experimentally is lower. The relationship between the elastic modulus and the crystallographic orientation of the testing direction is described by the following equation (11):

$$1/E = (C_{11}+C_{12})/(C_{11}-C_{12})(C_{11}+2C_{12}) - 2(1/(C_{11}-C_{12}))(\alpha_1^2\alpha_2^2 + \alpha_2^2\alpha_2^3 + \alpha_3^2\alpha_1^2) \quad \text{eq. 2.10}$$

C_{11}, C_{12}, C_{44} - elastic constants of cubic crystals

α_1, α_2, α_3 - direction cosines of particular crystallographic orientation

This equation predicts the highest modulus in a single crystal of aluminum to be in the [111] direction. The [111] direction is perpendicular to the plane with the closest packed atoms and therefore, the strongest interatomic binding. The lowest modulus is predicted to be in the [100] direction. The (100) plane contains atoms which are bound by secondary interatomic bonds which are weaker. Using the elastic constants from Kittel (12), the ratio of the maximum and minimum elastic moduli for single crystal aluminum results

in the following:

$$E_{111}/E_{100} = 1.2 \quad \text{eq. 2.11}$$

The difference in modulus between two crystallographic directions cannot exceed 1.2 in aluminum. However, the presence of alloying additions in solid solution or as secondary phases may increase or decrease the dependence of the moduli on crystallographic orientation.

2.1.4 Measurement Techniques

There are two different methods used to determine the elastic moduli. There is a static technique and a dynamic technique. The static technique involves applying a load to

a sample within the elastic limit and measuring the strain as a function of the applied load. An extensometer or strain gauge is used to monitor the strain. The modulus is measured as the slope of the linear region of the stress strain curve. This type of method requires great experimental care to be precise. The mechanical alignment must be closely monitored. High-precision strain gauges must be properly attached to the specimen. The static method allows time for thermal or atomic diffusion as mechanisms for relaxation to occur. Static measurements are obtained under isothermal conditions. During testing there is enough time for the sample to maintain thermal equilibrium with the surroundings. Also, when using this method, aluminum may exhibit microplasticity at low elastic strains. The static method usually gives a lower value for the modulus due to the above mentioned reasons.

There are two commonly used dynamic techniques: the resonance technique and the pulse echo technique. The use of these ultrasonic techniques is widespread. The resonance technique uses a specific geometrically designed sample and measures the resonance frequency of the vibrating sample. The pulse echo technique measures the velocity of ultrasonic waves in a sample. The second technique was used in this investigation. The original method described by Huntington (29) and several variations of this method are well established as a means for moduli determination.

The dynamic methods are more accurate for modulus measurement. The pulse echo method can be performed on small single crystal specimens cut along specific crystallographic directions and on polycrystalline materials. Very small atomic displacements and low stresses are used with the dynamic techniques. The strain cycles produced in dynamic testing occur at frequencies in the kHz to MHz range. The measurements are obtained under adiabatic conditions. There is no time for thermal equilibrium to be reached with the surroundings, therefore, the temperature of the specimen increases a small amount. The dynamic methods are also more attractive because they are nondestructive and more cost effective (30).

The pulse echo technique is based upon measurement of the time which elapses between the initiation and receipt of a pulse through a specimen. The ultrasonic pulse is created by an oscillating electric field, applied for several microseconds to a transducer which transforms the electric pulse into mechanical motion. When applied to a single crystal material the velocities obtained in the different crystallographic orientations can be used to calculate the elastic constants of the material. When applied to a polycrystalline sample the velocities measured are used to calculate the overall elastic moduli. A large amount of the ultrasonic moduli determination has been reported for single crystal materials where the elastic constants were directly measured (31). However, ultrasonic

characterization has been performed on a variety of other materials including polycrystalline alloys and metal matrix composites (32,33,34). Zimmer and Cost (35) used ultrasonic methods to perform the first study of the elastic constants of a unidirectional fiber composite material. Thomas et al. (36) used the pulse echo technique for determining small changes in the Young's modulus.

2.2 Phases in Aluminum Alloys

J.M. Silcock studied the precipitation sequence of aluminum-lithium alloys in 1959 (37). The precipitation sequence is as follows:

$$SSSS \text{ ------ } \delta' \text{ ------ } \delta$$

SSSS is the supersaturated solid solution. Delta prime δ' (Al_3Li) is an ordered metastable phase. Delta δ (AlLi) is the stable equilibrium precipitate. The accepted binary phase diagram (38) is given in figure 2.

The equilibrium delta phase is partially coherent with the matrix. It usually nucleates heterogeneously along grain boundaries and is detrimental to the mechanical properties.

The metastable delta prime phase is the primary strengthening precipitate in aluminum-lithium alloys. The precipitation characteristics of the delta prime phase have been examined by Noble and Thompson using transmission electron microscopy (39). The coherency of the delta prime precipitate has been investigated by D.B. Williams and J.W. Edington (40). Both investigations report the

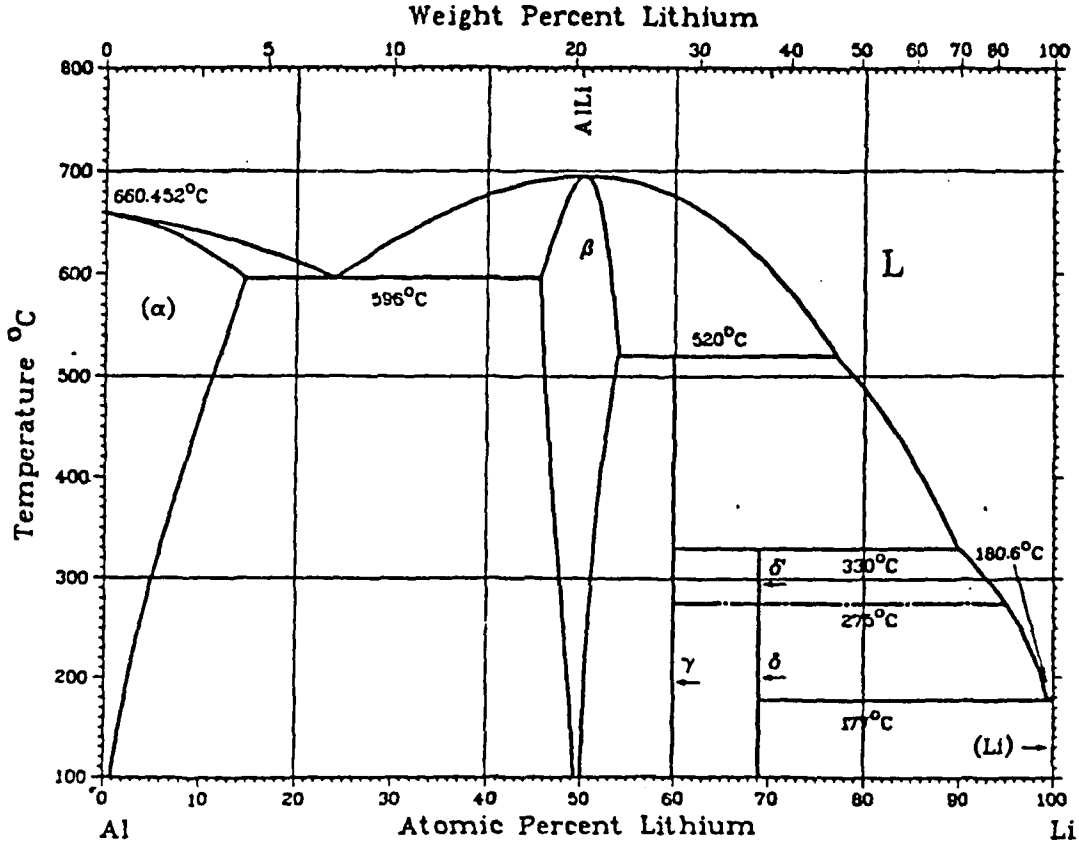

Figure 2. Aluminum-Lithium binary phase diagram (38).

presence of the delta prime phase upon quenching low lithium containing aluminum alloys from the solid solution temperature range. The delta prime phase has a $L1_2$ superlattice crystal structure and forms as spheres with a cube/cube orientation relationship with the matrix. Recently, several researchers have suggested that a miscibility gap may exist below the delta prime solvus. Nazoto and Nakai (41) propose that GP zone phases and a short-range ordered phase precedes the delta prime phase. Papazian et al.(42) predict a miscibility gap using theoretical calculations and differential scanning calorimetry. They predict a phase with kinetics which are similar to Guinier Preston zones in other aluminum alloys. The precipitation mechanism by which delta prime forms may be either spinodal decomposition (42,43) or coherent nucleation and growth (24). The mechanism has not been definitely established. It has been shown (44) there are no apparent differences between the delta prime coarsening rate in the binary and ternary alloys.

Delta prime is a coherent precipitate and possesses a low lattice misfit with the matrix (45). Due to the low interfacial energy between the delta prime phase and the matrix phase, the delta prime phase nucleates homogeneously. The lattice mismatch of the delta prime phase is estimated to be -0.08% (39). Several researchers (46, 69) believe, because the delta prime has such a good fit with the matrix,

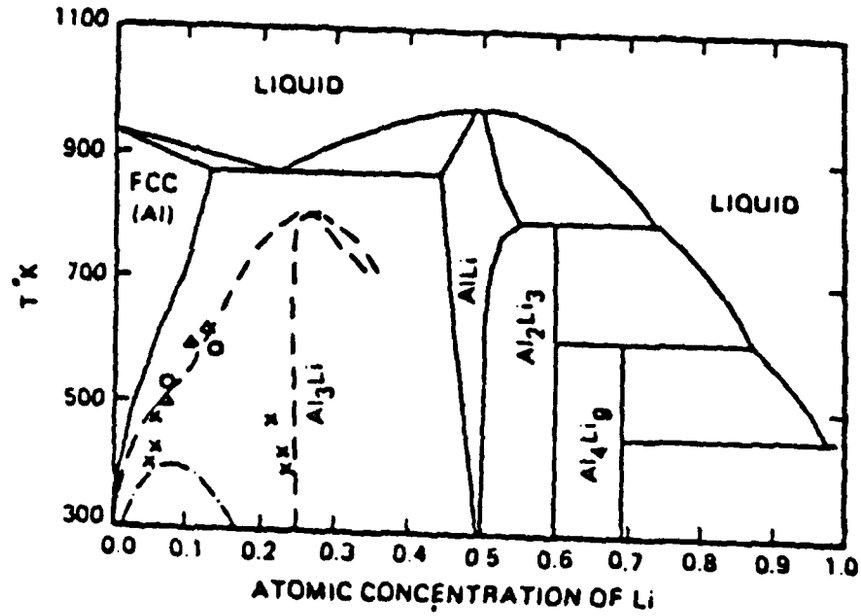

Figure 3. Aluminum-Lithium phase diagram illustrating the miscibility gap which is theoretically predicted by Sigli and Sanchez (42).

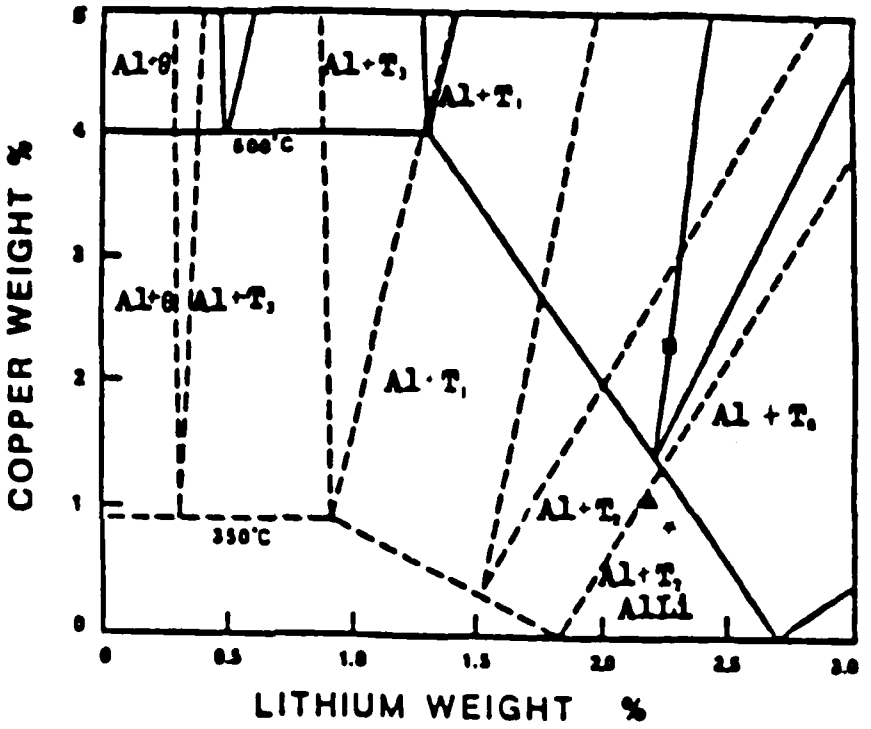

Figure 4. Isothermal sections calculated at 350 C and 500 C for the Aluminum-Copper-Lithium system (49). The ternary experimental alloys are indicated by the following symbols: ■ Alloy 73, • Alloy 81, ▲ Alloy 82

A typical precipitation sequence for a high copper containing Al-Li alloy is the following:

SSSS---- GP zones ----θ''----θ'---- $\theta(Al_2Cu)$
`---- T1(Al_2CuLi)

In addition to the phases typical of Al-Li and Al-Cu alloys six ternary intermetallic compounds were found in equilibrium at 500 C. They are the following: T1 (Al_2CuLi), TB ($Al_{7.5}Cu_4Li$), T2 (Al_6CuLi_3),P,Q, and R (Al_5CuLi_3). The compositions of P and Q have not yet been determined.

H.K. Hardy has shown that the addition of copper increases the strength of aluminum-lithium alloys while not decreasing the ductility (50). Copper improves the strengtn of aluminum-lithium alloys through solid solution and precipitate strengthening. According to Sainfort and Guyot (51), copper causes the peak aged condition to occur at an earlier aging time. In addition, copper may contribute to a more homogeneous distribution of the Al_3Zr phase.

The precipitation sequence in aluminum-zirconium alloys is the following:

SSSS----Al_3Zr (metastable cubic)----Al_3Zr (metastable tetragonal)

The metastable Al_3Zr precipitates have an $L1_2$ crystal structure and a cube/cube orientation relationship with the matrix (52). When zirconium is added to aluminum-copper-lithium alloys zirconium forms a cubic Al_3Zr coherent dispersoid. Due to the very low solubility of zirconium in the alpha matrix, Al_3Zr is always present after solution

heat treatment. At 427 C the solid solubility of zirconium in aluminum is between 0.05 and 0.06 at% (53).

The addition of zirconium has several effects. Recrystallization is inhibited during alloy processing. This is favorable to maintain a fine grained microstructure. Zirconium additions also afford superplastic properties and provide strengthening. Gu et al. have shown that the addition of zirconium accelerates the aging kinetics of delta prime (54).

Work by W. Stimson and D.B. Williams (55) supports there is negligible chemical interaction between lithium and zirconium in either the precipitates or in the matrix. Makin and Ralph (56) indicate that the chemical interaction between lithium and zirconium is negligible in either the precipitate or matrix. However, the detection of lithium in aluminum-lithium alloys is difficult. The characteristic x-ray wavelength of lithium is 220 angstroms. It is usually absorbed before it can be detected. Research done by F.W. Gayle and J.B. VanderSande indicates that there is interaction between the lithium and zirconium (57). The extent of the interaction between the lithium and the Al_3Zr has not been quantitatively established. Commonly, the Al_3Zr dispersoid particles found in these alloys, are surrounded by Al_3Li which nucleates preferentially at the interface. T. Malis (58) performed EDS and EELS analysis of these coated spherical configurations. Malis confirmed that both zirconium and lithium were present in the cores

and that Al_3Li surrounded these cores.

It is evident that a variety of phases exist in the aluminum-copper-lithium alloy systems. Each phase has a different contribution to the overall elastic behavior of the alloy.

Chapter 3

EXPERIMENTAL PROCEDURE

3.1 Alloy Material

The alloys investigated were manufactured by Reynolds Metals Company, Richmond, Virginia. The material was received as hot cross-rolled plate with a thickness of 12mm. Three aluminum-copper-lithium alloys and one aluminum-lithium binary alloy were examined.

All the alloys were solution heat treated at 550 C for 30 minutes in a salt bath and cold water quenched (CWQ). The chemical analysis was performed on the alloys in the solution heat treated condition and after aging for 100 hours at 190 C in an air convection oven. There was not a significant loss of lithium during the aging treatments at 190 C. Luvak Incorporated performed the chemical analysis. Alloy 73 is similar in composition to Alcoa's 2090 commercial alloy. Alloys 81 and 82 have a lower copper to lithium ratio. The compositions are given in Table I.

All samples, alloys 73, 81, 82 and the binary alloy, were aged at 190 C for times from 10 minutes up to 300 hours. Alloy 73 was examined in the stretched and unstretched condition. The stretched alloy was aged at 190 C and 300 C.

Stretching is of commercial importance in copper containing aluminum-lithium alloys because it enhances

Table I. Alloy Compositions

ALLOY	Al	Cu	Li	Zr	Cu/Li ratio
wt% / at%					
73	94.79 / 90.55	2.24 / 0.90	2.31 / 8.51	0.16 / 0.04	0.97 / 0.11
81	96.32 / 90.51	1.07 / 0.43	2.47 / 9.02	0.14 / 0.04	0.43 / 0.048
82	96.64 / 91.54	1.06 / 0.43	2.17 / 7.99	0.13 / 0.04	0.49 / 0.054
Binary	97.85 / 92.599		2.00 / 7.36		
Alcoa's 2090	94.78 / 90.684	2.70 / 1.10	2.20 / 8.19	0.12 / 0.03	1.23 / 0.13

ductility. The stretched material demonstrates the effect of an increased density of dislocations and point defects on the microstructure, hence on the elastic modulus. An increased amount of defects within the matrix provides for an increased number of nucleation sites for copper containing precipitates and therefore, precipitation within the matrix. This is desirable for several reasons. A shorter aging time can be used to attain the desired volume fraction of precipitate. There will be less precipitation of AlLi along the grain boundaries and therefore, an improvement in ductility.

The 300 C aging temperature was examined in order to specifically examine the contribution of the T1 phase to the modulus. 300 C is above the solvus temperature for the delta prime phase. Density measurements, velocity measurements, length measurements, elastic modulus, shear modulus, and Poisson's ratio calculations were made after each of the aging times and conditions.

3.2 Sample Preparation

The solution heat treatment temperature was sufficient to get all of the elements into solution except the zirconium containing phase (Al_3Zr) and small amounts of iron and silicon impurities.

Some of the samples were stretched to a plastic strain of 6% under uniaxial tension using a MTS closed loop loading apparatus.

All the alloys were machined into appropriate specimens for ultrasonic measurement in the solution heat treated and CWQ condition. All samples were taken from the center of the plate.

The ultrasound samples had different geometries. The rectangular samples were approximately 12mm X 7mm X 5mm. The cylindrical samples were 6 to 9mm in diameter and 7 to 11mm in height. A variety of geometric configurations was used to insure the geometry of the samples did not influence the pulse echo measurements. Samples were prepared from the short transverse, long transverse and longitudinal directions.

3.3 Pulse Echo Measurement

Ultrasonic measurements were taken in the short transverse, long transverse and longitudinal directions.

The acoustic wave velocities were measured by the direct ultrasonic pulse-echo technique. The experimental set up is comprised of an Ahrenberg pulsed oscillator model PS-660, an Ahrenberg #455 attenuator, a balancing network, an Ahrenberg wide band amplifier model WA-600-E, and a Tetronix oscilloscope model 2236. A schematic of the experimental set up is given in figure 5, p.33. Dow resin, poly-α-methyl-styrene, was used to affix 10 MHz quartz transducers to each sample. It transmits shear and longitudinal waves. The transducer detects the initiation and receipt of the pulse. 10 MHz pulses were sent from the pulsed oscillator. A pulse

duration of 1 millisecond and a pulse repetition frequency of 10 microseconds were used. The attenuator controls the size of the pulses. The balancing network matches impedances between the quartz crystal and the pulse. The network allows modification of the main pulse so that the best echo pattern is obtained. X-cut quartz crystals were used to obtain longitudinal velocities; Y-cut quartz crystals were used to obtain transverse velocities. The quartz crystals used were all 6mm in diameter with a thickness which allowed for a 10MHz resonance.

The samples were polished so that the sides were parallel. This is critical to get a usable pulse echo pattern. Specimen length measurements were made using a standard micrometer.

Velocities were calculated for the longitudinal and transverse waves. The following equation was used (19):

$$V = t/2L \qquad \text{eq. 3.1}$$

V - velocity
t - distance between echoes
L - Sample length (mm)

The most consistent and reproducible pulse echo patterns were used. At least five equal pulse lengths were observed in each direction. Usually, more were observable. The elastic modulus, shear modulus, and Poisson's ratio were calculated. The following equations were used (18):

$$R = (V_t/V_l)^2 \qquad \text{eq. 3.2}$$

$$P = (2*R-1)/(2*R-2) \qquad \text{eq. 3.3}$$

$$G = V_t^2 * D \qquad \text{eq. 3.4}$$

$$E = D * V_l^2 * ((1+P)*(1-2*P)/(1-P)) \qquad \text{eq. 3.5}$$

R - Ratio of velocities squared
P - Poisson's ratio
G - Shear Modulus(GPa)
E - Elastic Modulus (GPa)
D - Density(g/cc)
V_t - Transverse velocity (m/sec)
V_l - Longitudinal velocity (m/sec)

3.4 Density Measurements

All samples were polished down to a 1 micron alumina finish on all sides. After polishing, samples were cleaned in acetone using an ultrasonic cleaner. This step was essential for accurate density measurements. The smooth polished surface prevented the formation of air bubbles on the sample surface when the samples were weighed in liquid. Density measurements were performed using a technique based upon Archimedes' principle. Samples were weighed using a Mettler electronic balance, which gave readings accurate to ten thousandths of a gram. The samples were weighed in air and, suspended from a thin copper wire, in carbon tetrachloride. The temperature of the CCl_4 was taken after every measurement. Temperature readings were accurate to a tenth of a degree celcius. The density of the CCl_4 was adjusted according to the temperature. All measurements were performed in a controlled air environment. A standard aluminum specimen with a stable microstructure was measured along with each experimental sample. All measurements were

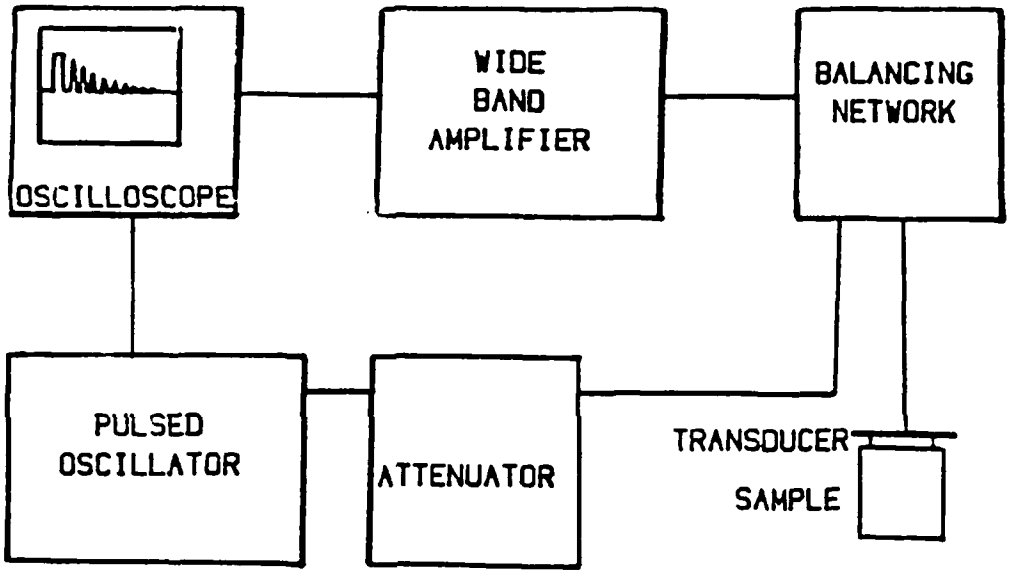

Figure 5. Schematic of the Pulse Echo measurement system.

normalized with respect to the standard specimen. The amount of error found for the standard sample using this technique was 0.016%. This is within reason for our analysis.

Density was calculated using the following equation (18):

$$D = W*C/(W-V) \qquad \text{eq. 3.6}$$

D - Density of sample (g/cc)
W - Weight of sample in air (g)
C - density of CCl_4 (g/cc)
C=f(T) (59)
V - Weight of sample in CCl_4 (g)
T - Temperature of CCl_4

3.5 Texture

Texture analysis was performed in order to examine the effect of orientation upon the modulus in polycrystalline alloys. Pole figures were obtained using a Siemens texture goniometer, set up for the Schulz reflection technique. Cu K_α radiation was used. A pole figure represents the preferred crystallographic orientations (texture) of a polycrystalline material, with reference to a standard stereographic projection. Pole figures were obtained for all samples in the solution heat treated and CWQ condition. Samples were machined as rectangular specimens, 50mm X 40mm X 2mm. They were taken from the center of the plate with the broad surface parallel to the rolling surface. The sample surface was polished down to a 1 micron alumina finish. Deformation layers were etched away using a solution of 10 grams NaOH and 90ml of water at 60 C. They were rinsed in diluted

HNO_3.

The diffracted x-ray intensities from (hkl) planes were collected on a goniometer by rotating the specimen around the short transverse direction (0-360°) and the long transverse direction (0-70°). A computer program organizes and analyzes these data. Pole figures are constructed from these data in the form of equal value contours and provides average, maximum and minimum intensities normalized with respect to a random sample.

3.6 Transmission Electron Microscopy

Transmission electron microscopy was used to identify the type of precipitates present, their volume fraction, and to examine the subgrain structure. A Phillips 400 (120KeV) electron microscope was used. Samples were electropolished using a Tenupol electropolishing unit. The electrolyte solution was a 4:1 methanol:nitric acid solution. The current density was 0.01 amps/mm^2 at 12 volts.

3.7 Small Angle X-ray Scattering

Small angle x-ray scattering is a valuable tool for determining the following: 1) the kinetics of precipitation, 2) the onset of growth or coarsening, 3) particle size distribution, and 4) volume fraction of second phases.

SAXS experiments were performed at the National Laboratory at Oak Ridge, Tennessee. Cu K_α radiation was used. Data was collected at sample to source distances of 5 meters and 3 meters from sample to source. The theta angles

examined were from 0.010 to 0.695 degrees. Alloys 73, 81 and 82 were examined at different aging times. Samples were prepared as 3mm diameter discs. The discs were punched out after mechanical thinning to about 0.05mm thickness. They were then electrolytically thinned using a 4:1 methanol:nitric acid solution at -15 C. The final thickness was approximately .007mm.

SAXS does not give structure identification but it gives information from an volume greater than 10 um^3, which is more representative than the small volume examined by TEM.

3.8 Guinier X-ray Examination

Guinier x-ray examination is a useful tool for identification of second phases and determining their volume fractions. The Guinier x-ray examination identifies which phases are present due to the position of the reflections which are recorded on the film. The relative volume fractions of the different types of precipitates are measured by examining the intensities of the reflections on film. This is performed using a microdensitometer.

Samples were cut, mechanically thinned to approximately 200 microns and electrolytically thinned to 70 microns in thickness. The electrolytic solution was 4:1 methanol to nitric acid. A Huber Guinier Camera with a quartz monochromator using Cu $K\alpha_1$ radiation was used in this investigation. Samples were examined in the transmission mode. A typical exposure time was 24 hours.

A microdensitometer made by Joyce, Loebl & Co., England was used to examine the x-ray film. This device measures the amount of photographic density of the film by sending a beam of light through the film and comparing it with a reference light beam from the same source. The photographic density of the film is related linearly with the x-ray intensity. A plot of the amount of blackening versus 2θ is equal to the intensity versus 2θ .

The integrated intensity is the area under the intensity versus 2θ curve and is also proportional to the volume fraction of the phase causing the diffraction peak. The second phases are identified at specific peaks.

The ratios of the integrated intensities for second phase peaks and an aluminum matrix peak were used to determine volume fractions of second phases.

3.9 Optical Metallography

Optical metallography was performed in order to examine the grain structure and large inclusions. Samples were polished down to a 1 micron alumina finish and etched using Kellers reagent. Photomicrographs were taken using a Zeiss optical microscope model MC63A.

3.10 Scanning Electron Microscopy

The scanning electron microscope is useful for examining surfaces and microstructures. When it is used in conjunction with an energy dispersive x-ray analyzer (EDAX)

it is useful to examine chemical compositions of specific features. An analytical scanning electron microscope, Jeol model 35, was used to examine the large inclusions in the alloys investigated. An EDAX was used to identify the elements present in the inclusions. SEM analysis indicates that the amount of iron and silicon was negligible.

CHAPTER 4

RESULTS

4.1 Microstructure

The microstructures of alloys 73, 81 and 82 were examined using optical microscopy and transmission electron microscopy. The binary alloy was examined in previous work (60). It has a fully recrystallized, equiaxed grain structure with an average size ranging from 340 to 360 um. The optical micrographs of alloys 73 and 31 are shown in figure 6. They depict the grain structure in the short transverse, long transverse and longitudinal directions. This figure displays the elongated grain structure present in all three alloys. The grains are equiaxed in the rolling plane with an average diameter of 100 um. On longitudinal and transverse planes the grains are approximately 220 um X 33 um. The elongated grain structure is due to the hot cross-rolling of the plate during processing. The cross rolling of these alloys was performed at a temperature between 450 and 500 C.

TEM micrographs of alloys 73, 81 and 82 are given in figure 7. The typical unrecrystallized grain structure is present in all three ternary alloys. Zirconium containing dispersoids also show up due to strain field contrast. These fine Al_3Zr particles are obstacles to subgrain and grain boundary movement and thus, they inhibit recrystallization.

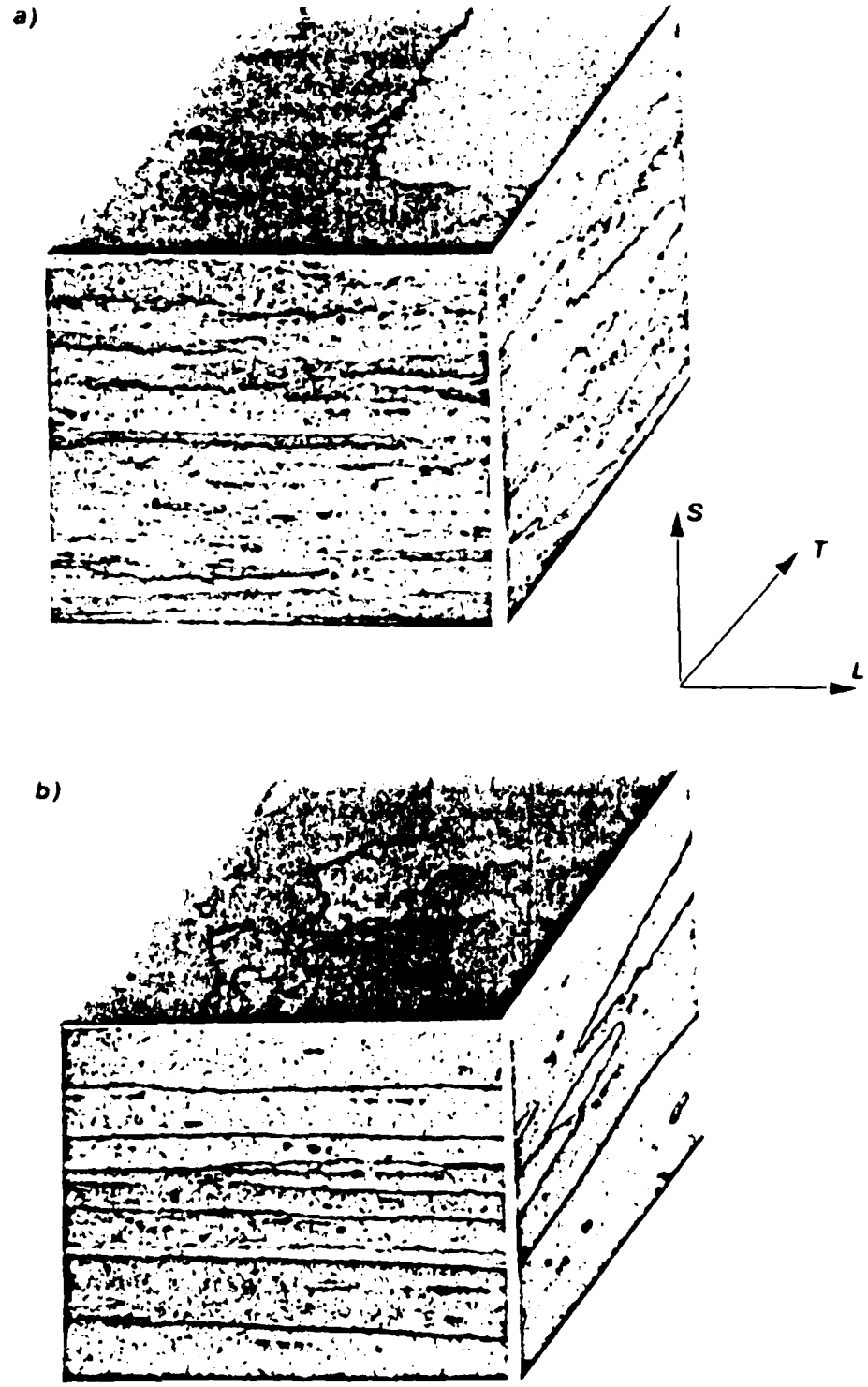

Figure 6. Optical micrographs displaying grain structure. a) Alloy 73 b) Alloy 81

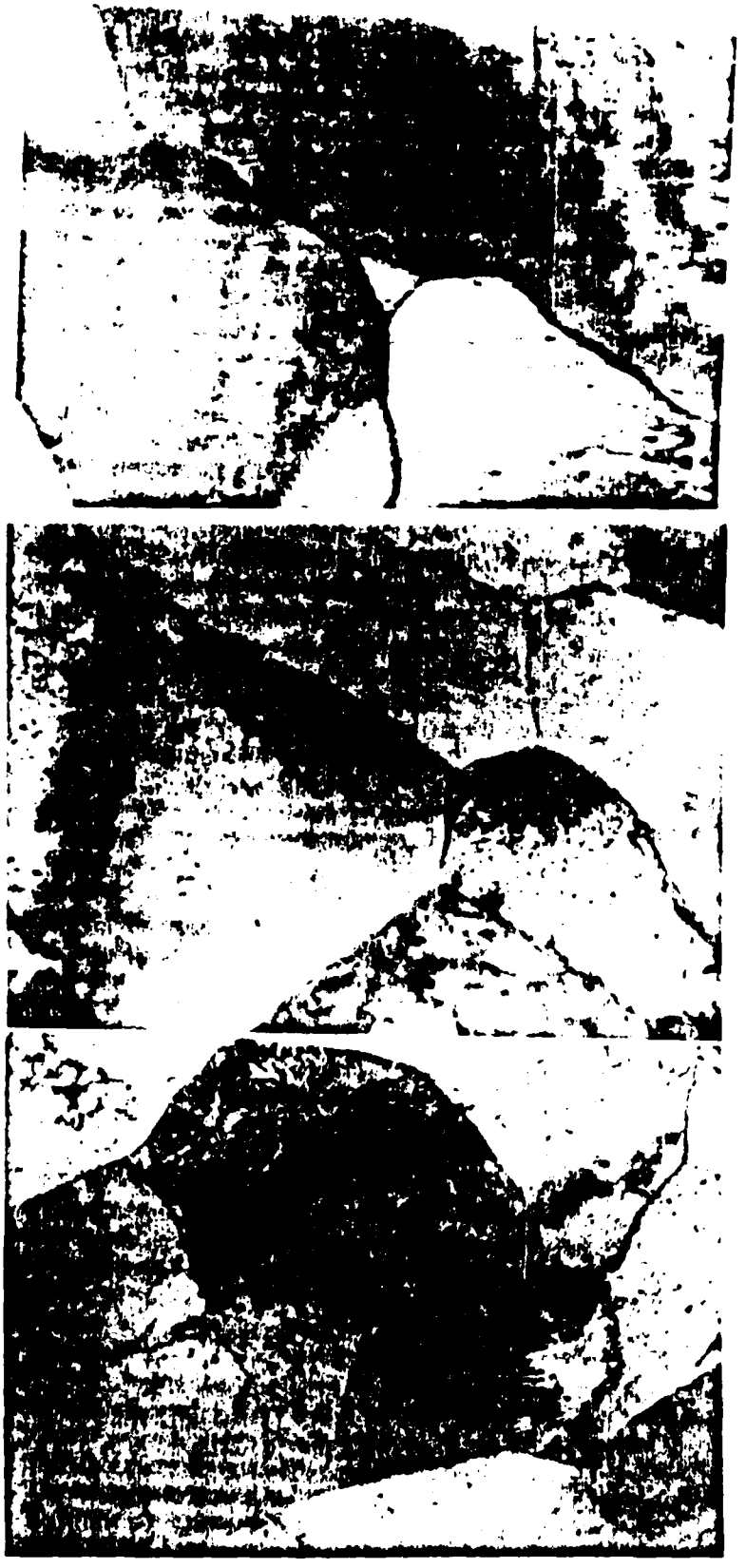

Figure 7. TEM micrographs displaying subgrain structure. a) Alloy 73, b) Alloy 81 and c) Alloy 82.

This subgrain structure is not present in the binary alloy.

In the solution heat treated condition the matrix, delta prime phase and Al_3Zr dispersoids were evident in the ternary alloys. Figure 8a is a TEM micrograph of alloy 73, solution heat treated, aged at room temperature for 2 weeks, which displays the delta prime phase, and Al_3Zr dispersoids. Figure 8b is a TEM micrograph of alloy 82, solution heat treated, displaying the Al_3Zr dispersoids. The diameters of the Al_3Zr dispersoids are approximately 20 nm. The delta prime precipitates have diameters of approximately 5nm. There was no evidence of other phases along the subgrain boundaries or grain boundaries. Guinier analysis of the solution heat treated condition showed the presence of the aluminum matrix and faint reflections from the superlattice positions of the delta prime phase. After ten minutes aging at 190 C, there is evidence of T1 precipitation in alloy 73. This was confirmed by both Guinier X-ray analysis and transmission electron microscopy. A TEM micrograph of alloy 73 after 10 minutes aging is given in figure 9. The T1 phase is found only at the grain boundaries and subgrain boundaries. The energy necessary for nucleation is less at the grain boundaries and subgrain boundaries. The T1 phase is plate shaped. It has less coherency with the matrix than the delta prime phase. Therefore, the T1 phase has a higher energy barrier to nucleation and will nucleate more favorably

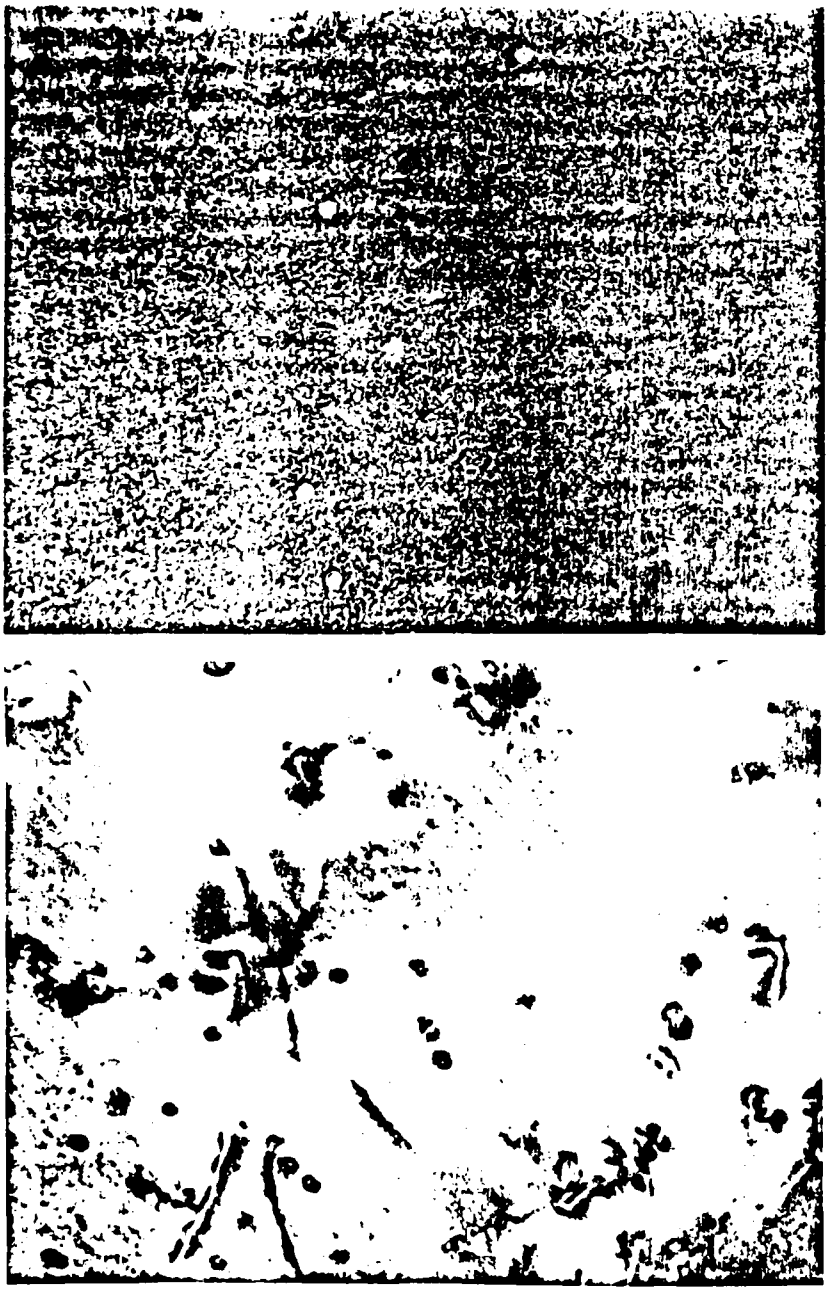

Figure 8. TEM micrographs: a) alloy 73, solution heat treated 30 minutes at 550 C. Micrograph displays delta prime and Al_3Zr. b) Alloy 82, solution heat treated 30 minutes at 550 C. Micrograph displays Al_3Zr.

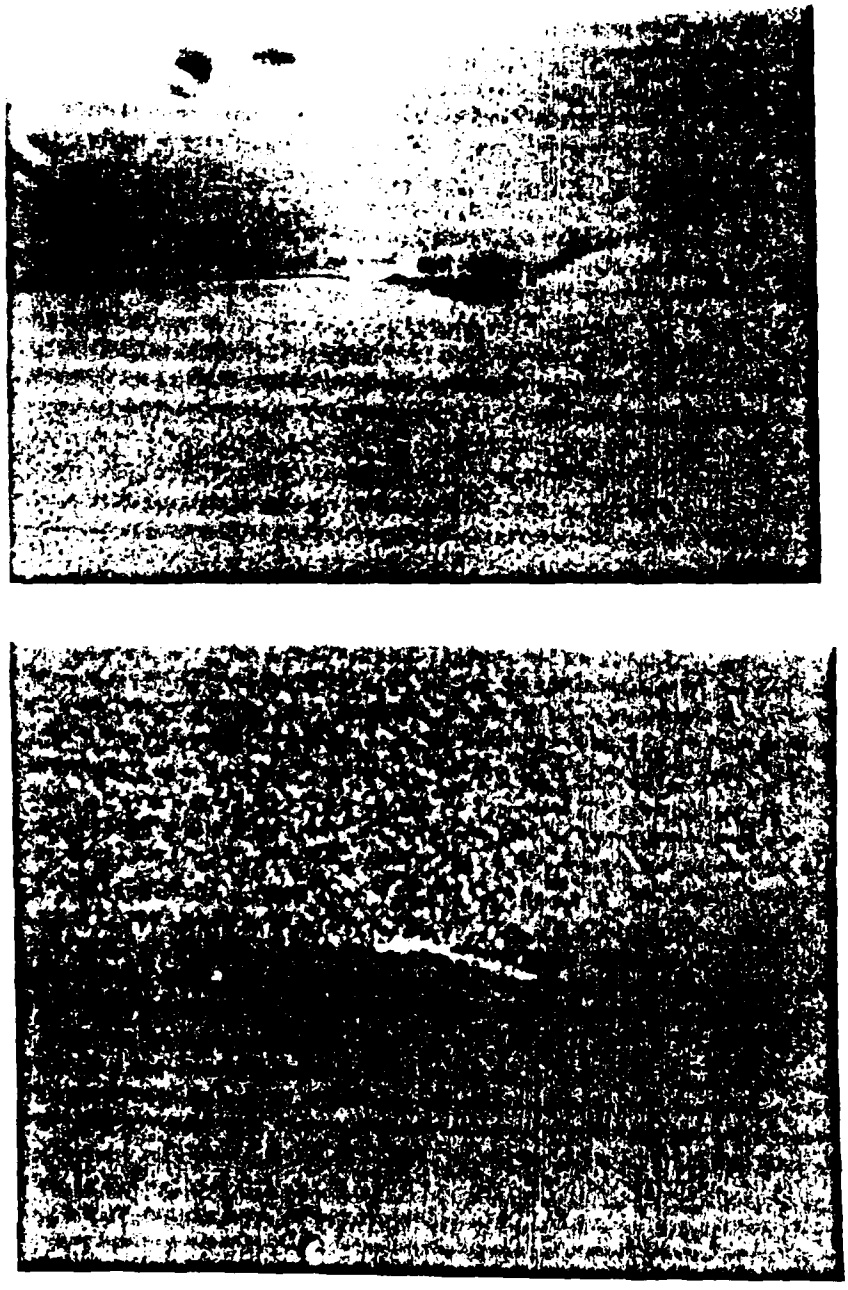

Figure 9. TEM micrographs of Alloy 73 after 10 minutes age at 190 C. The T1 phase is shown a) Bright field b) Dark field.

at the grain boundaries and subgrain boundaries. The T1 phase nucleates heterogeneously. The platelets, after 10 minutes aging at 190 C, are approximately 72 nm long and 8 nm wide. The delta prime phase is approximately 5.5 nm in diameter. The delta prime phase nucleates homogeneously throughout the matrix. It has a very good fit with the matrix. Therefore, it has a lower energy barrier to nucleation and its formation cannot be suppressed in the present alloys during cold water quenching.

Guinier analysis and TEM analysis give no evidence of the T1 phase in alloy 81 or 82 after 10 minutes aging. TEM micrographs of alloy 81 and 82 display the delta prime and Al_3Zr phases. Figure 10b shows the delta prime phase. Figure 10a displays a Al_3Zr particle surrounded by the delta prime phase. The delta prime phase has a diameter of approximately 5.2 nm in alloy 81 and 82 after 10 minutes aging at 190 C. This is slightly smaller than alloy 73. Alloys 81 and 82 are very similar in chemical composition. It is observed that these two alloys exhibit the same microstructures as the aging time varies.

After ninety minutes aging time at 190 C, the T1 phase is apparent in all three alloys (See figures 11 and 12). The amount present in alloy 73 appears to be greater. This may be due to the higher ratio of copper to lithium in alloy 73. The T1 platelets in alloy 73 are 300 nm long and 5.6 nm wide. They are approximately 67 nm long and 6.7 nm wide in alloys 81 and 82. Guinier analysis indicates that the

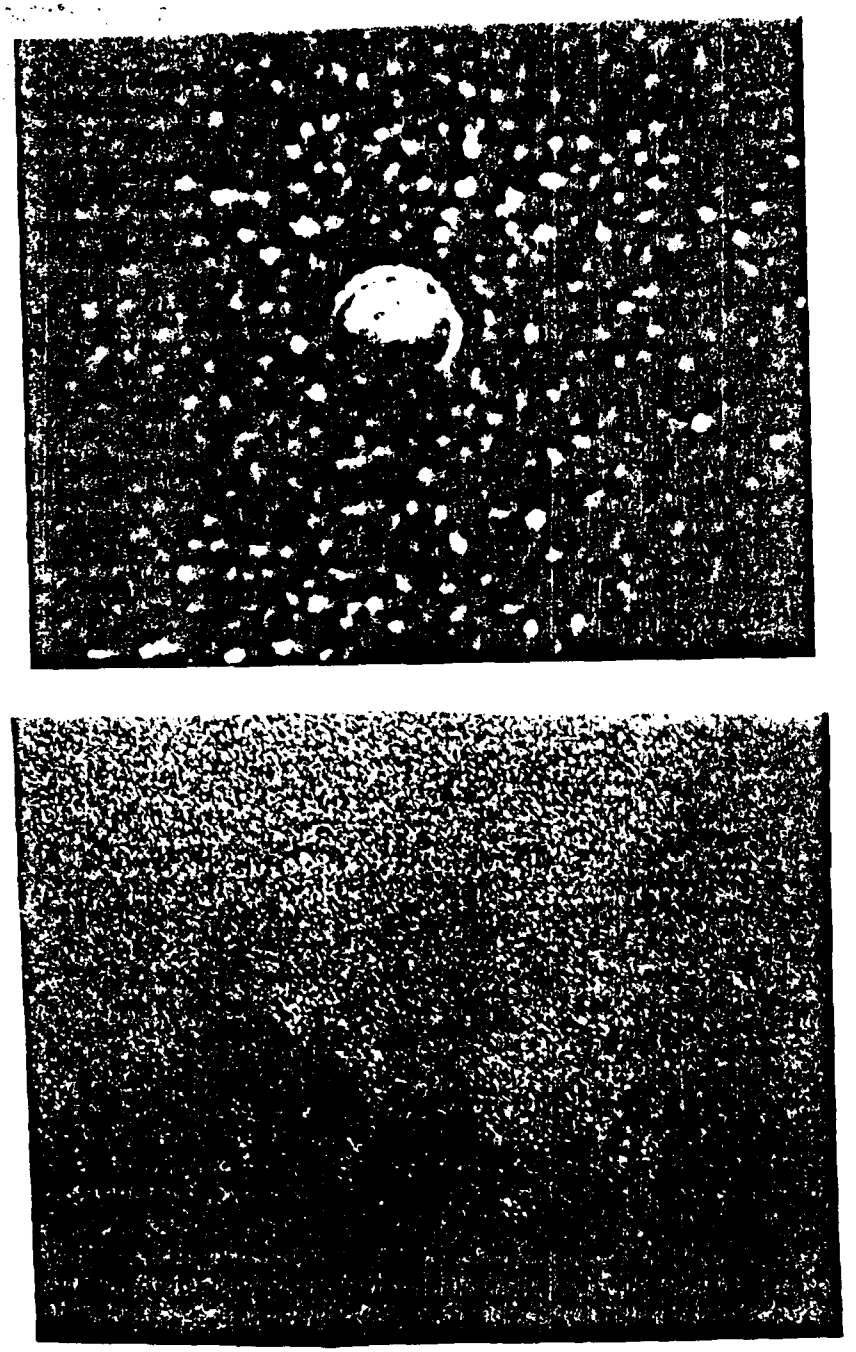

Figure 10. TEM micrographs of alloy 81 after 10 minutes age at 190 C. a) Dark field showing Al_3Zr particle surrounded by delta prime, b) Dark field showing delta prime.

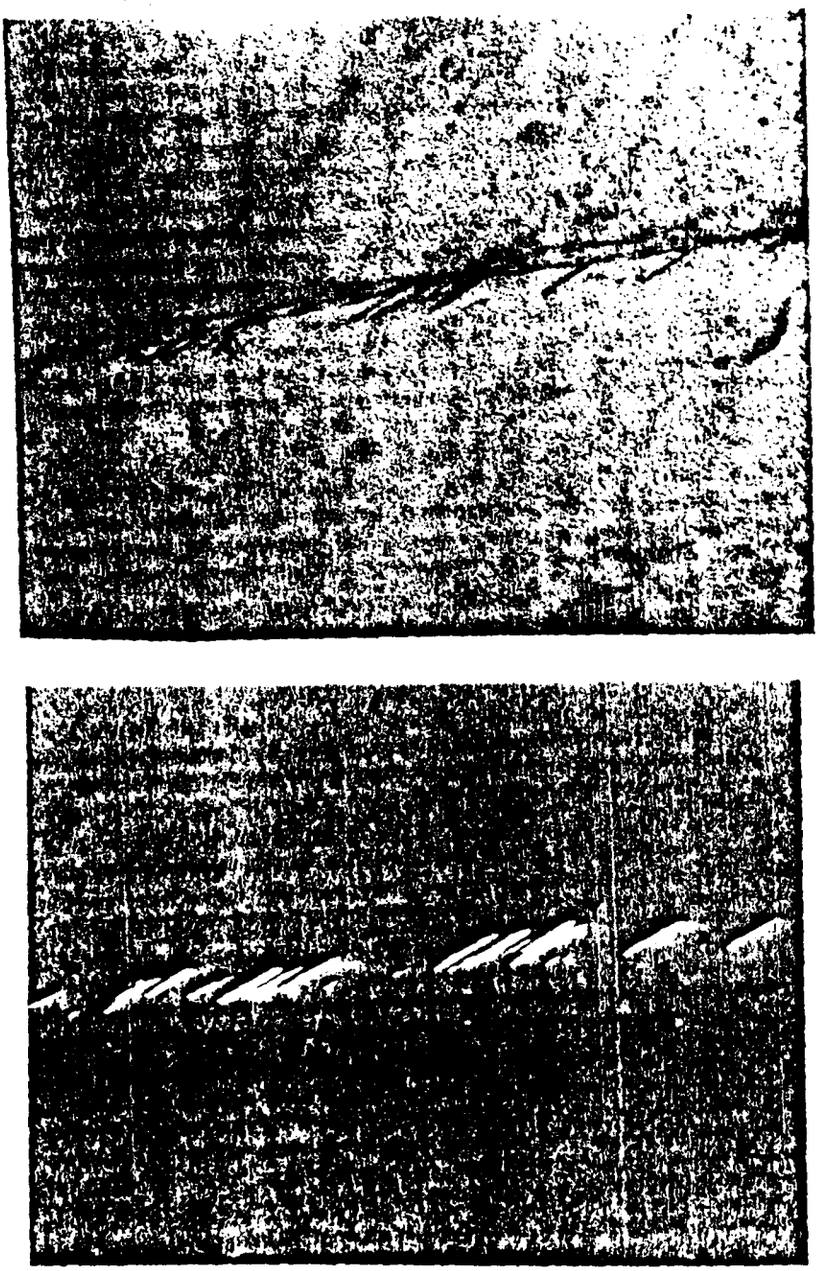

Figure 11. TEM micrographs displaying the presence of the T1 phase after 90 minutes aging time at 190 C, Alloy 73 a) Bright Field b) Dark Field

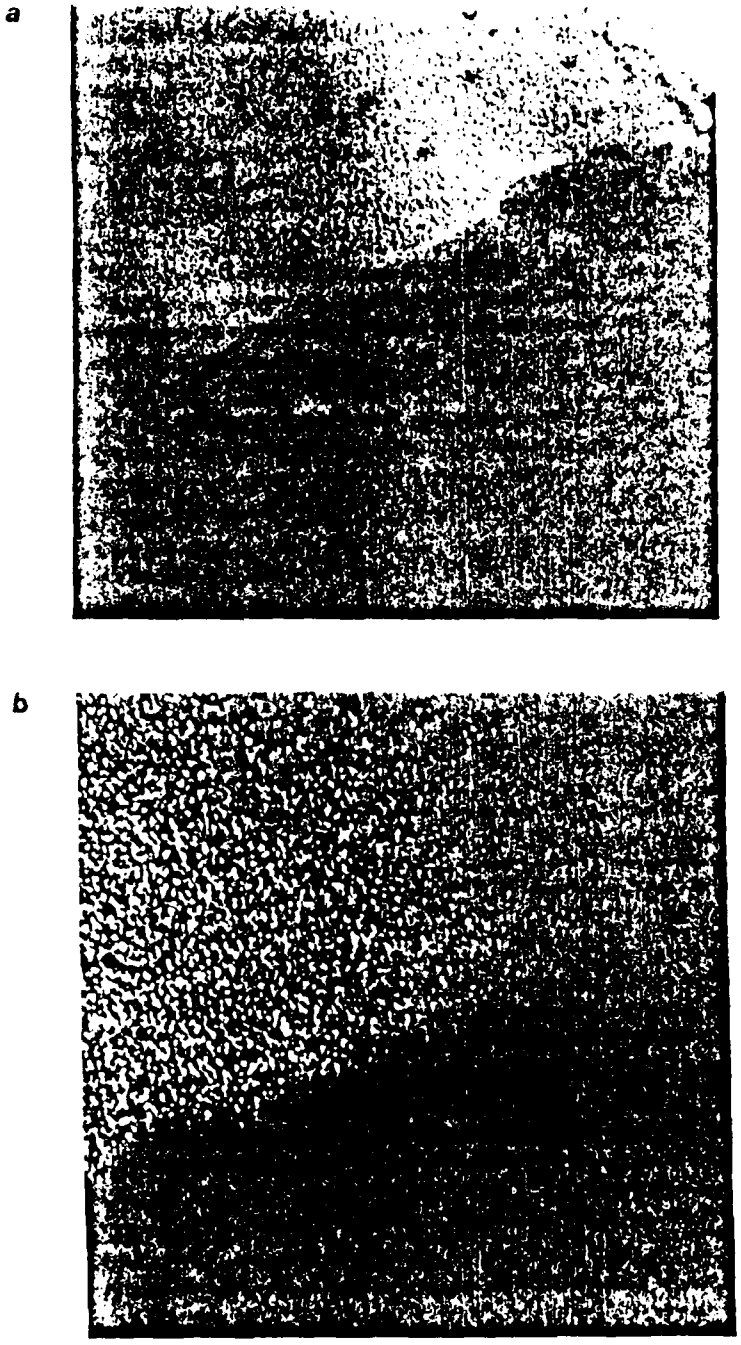

Figure 12. TEM micrographs displaying the presence of the T1 phase after 90 minutes aging time at 190 C, Alloy 81. a) Bright Field b) Dark field

intensity of the T1 reflections in the ternary alloys increases with increasing aging time. This indicates an increasing volume fraction of T1.

Alloys examined after four hours aging time were examined with the Guinier camera. There is evidence of the delta prime phase and the T1 phase. After 8 hours aging at 190 C, there is some T2 phase present in all three alloys. Faint lines indicative of the T2 phase are present on the Guinier film. TEM examination displays the T2 phase in the ternary alloys (See figure 13). The T2 phase nucleates preferentially along the grain boundaries. The T2 phase is energetically competitive with respect to the equilibrium phases in these alloys (61). Figure 13 also shows some T1 platelets in the matrix. Precipitate free zones are apparent at the grain boundaries (See figure 14). The PFZ's were not observed on the subgrain boundaries. The occurrence of second phases for the ternary alloys is summarized in figure 15.

The volume fraction of delta prime as a function of aging time was examined using TEM, SAXS and Guinier X-ray analysis.

TEM foils clearly showed the presence of delta prime. Foil thickness measurements were made using the convergent beam technique described by D.B. Williams (62). The volume fraction of delta prime was measured in alloys, which were aged for 8 hours at 190 C, using transmission electron

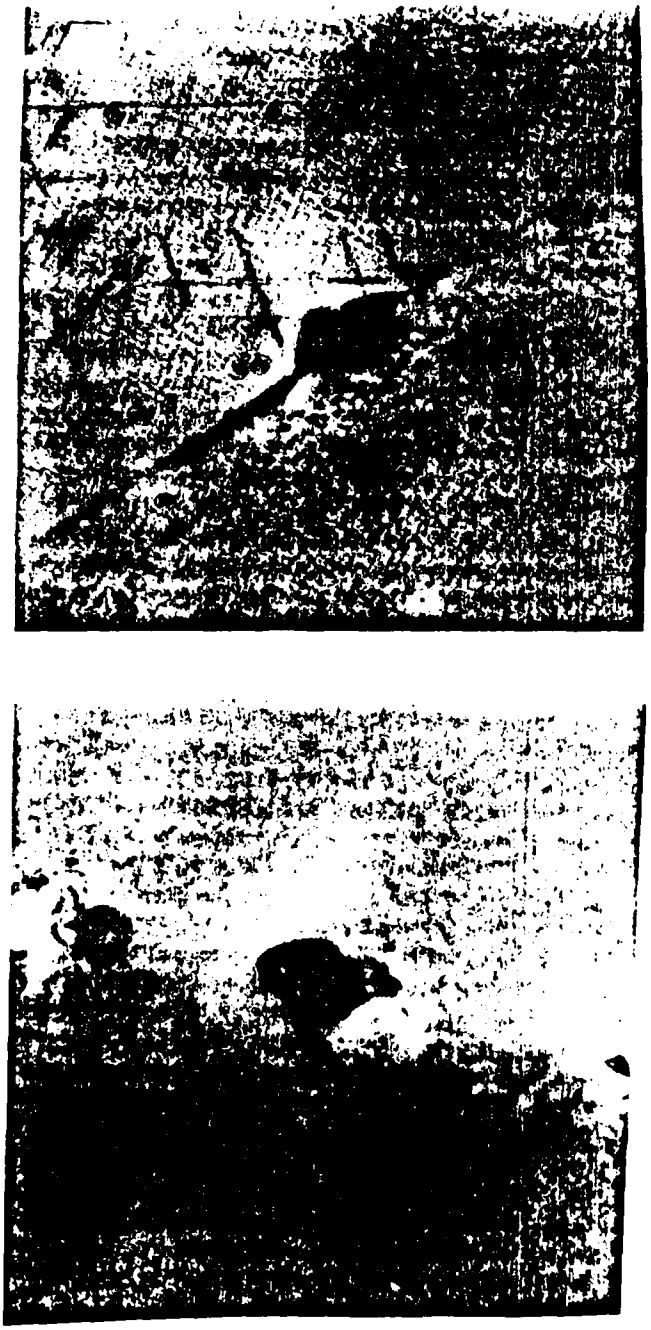

Figure 13. TEM micrographs displaying the presence of the T2 phase after 8 hours aging time at 190°C.
a) Alloy 73 and b) Alloy 81.

Figure 14. TEM micrographs displaying the T2 phase surrounded by PFZ in alloy 73 after aging 24 hours at 190 C.

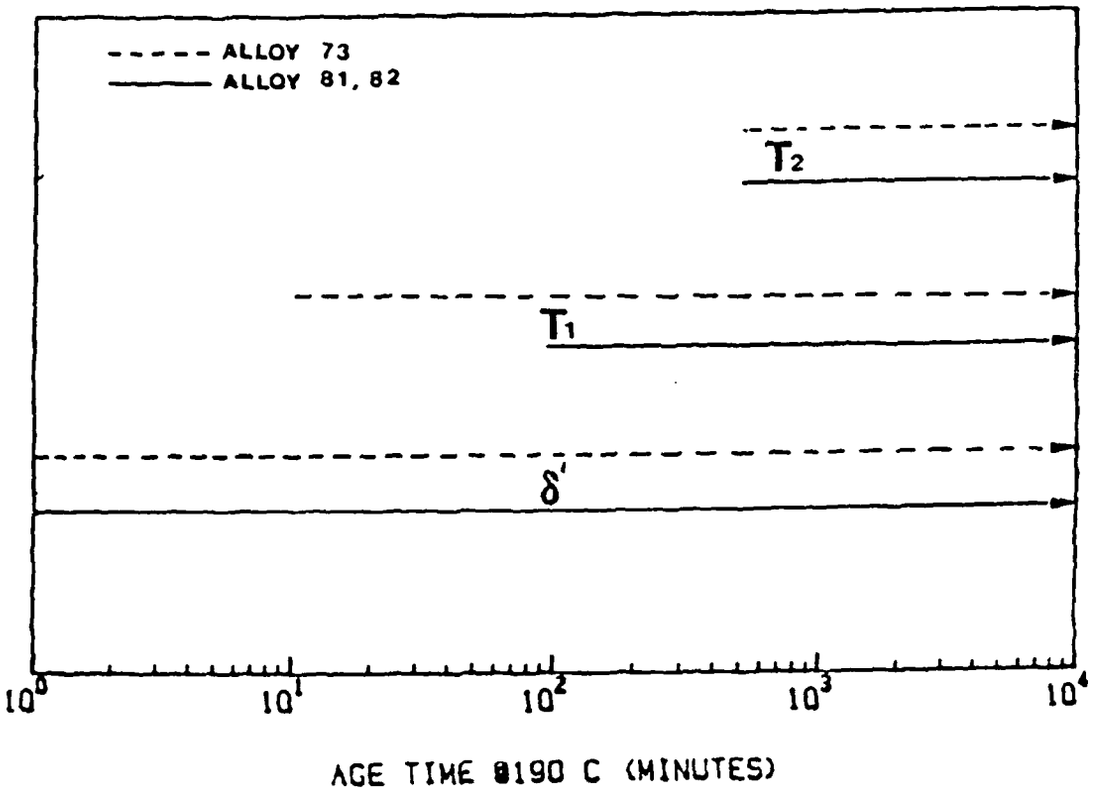

Figure 15. Profile of the occurrence of the delta prime, T1 and T2 phases in alloys 73, 81, and 82.

microscopy. The delta prime is not expected to deviate from spherical morphology (63). Therefore, spherical precipitates were assumed when calculating the volume fraction of delta prime. The equation which was used compensated for truncation and overlap (64). The volume fractions obtained from several measurements of the same alloy, different samples, are given in Table II. The volume fractions obtained using this method showed a large amount of scatter. This is primarily due to the difficulty in counting the spherical delta prime particles which frequently overlap and the difficulties in determining an accurate foil thickness.

Guinier x-ray analysis was also used to determine the volume fraction of delta prime for a specific aging time. The area of the (200) diffraction peak from the matrix phase and the (100) peak from the delta prime phase were measured. The intensity of the peak is proportional to the volume fraction of the particular phase, the structure factor squared, the Lorentz polarization factor, a multiplicity factor and an absorption coefficient. This simplifies to a proportionality between the ratio of the intensities of the matrix and delta prime and their respective volume fractions. Reflections from the same family of orientation were used, i.e. (200) and (100). The procedure used is described in more detail by H.P. Klug (65). The Guinier data taken from different samples of the same alloy is shown

TABLE II

Volume fraction of delta prime

Alloy	Age time at 190 C	TEM method	GUINIER method
		(vol%)	
Binary	200 hrs		12.7
Binary	200 hrs		12.6
81	4 hrs		11.2
81	8 hrs	7.0	
81	8 hrs	11.0	14.0
81	8 hrs	6.5	14.0
81	20 hrs		13.8
81	20 hrs		13.9
81	100 hrs		13.9
73	100 hrs		13.8
73	100 hrs		14.0
73	100 hrs		13.9

in Table II. The scatter for the Guinier volume fractions is much less than the TEM values. The percent scatter calculated for the Guinier technique is approximately 1%. The percent scatter calculated for the TEM technique is approximately 30%. Therefore, the values obtained from the Guinier technique were used.

SAXS analysis was performed at Oak Ridge National Laboratory. The analysis was used to determine relative changes in volume fractions as a function of aging time at 190 C. Only relative volume fractions were obtained because no calibration standard was available at the time the experiments were done. Kratky plots are indicative of the volume fraction of precipitates present. They are plotted as K^2*I versus K. I represents the intensity and K is the position vector; it is equal to $4\pi \sin\theta / \lambda$. Figure 16 shows a typical Kratky plot of alloy 81 after 100 hours of aging at 190 C. The area under the curve has been measured with a planimeter. The relative changes in volume fraction determined this way are plotted in figures 17 for alloy 81. A clear increase in the amount of precipitates with aging time can be seen.

The SAXS analysis also gave Guinier plots. These are represented by I versus K. The slope of the Guinier plots is indicative of the Guinier radius of the second phase. The particle radius is equal to the Guinier radius multiplied by 1.29099. In alloy 81 the particle radius,

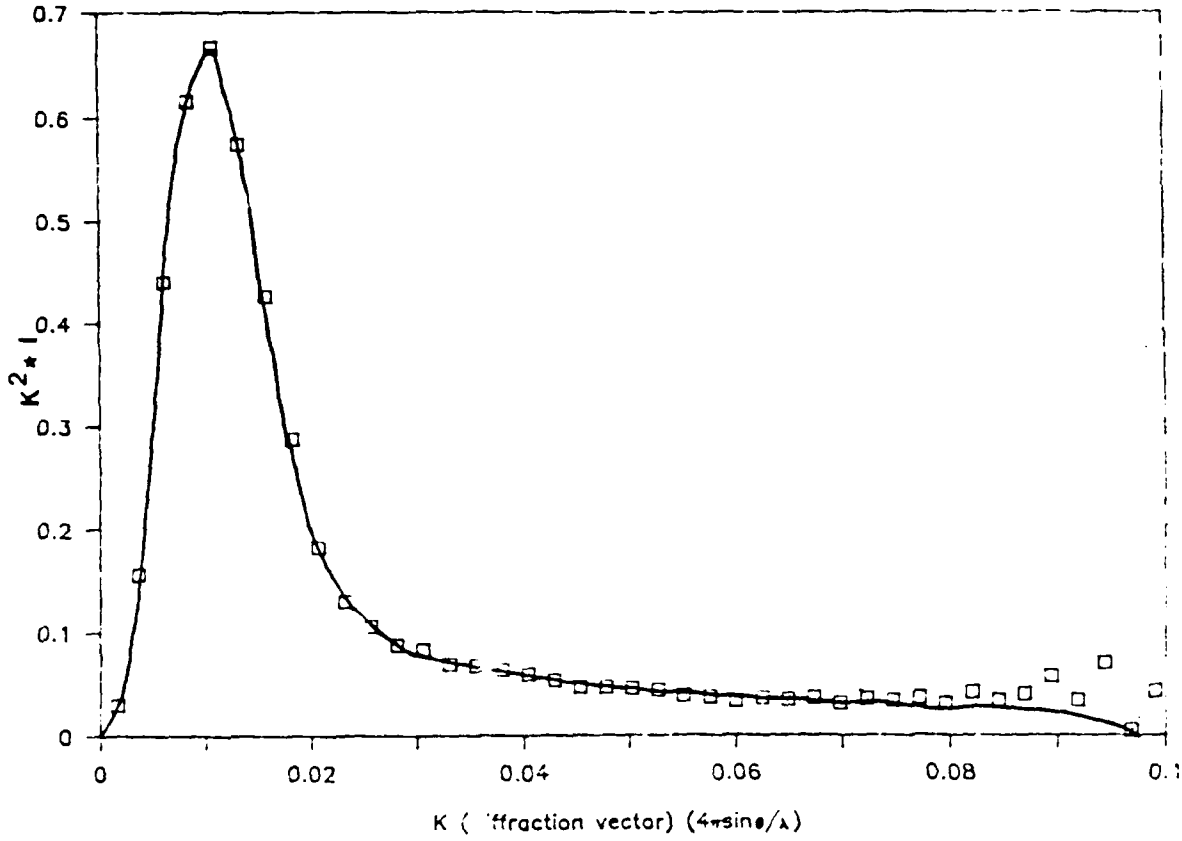

Figure 16. Sample Kratky Plot for alloy 81 after 100 hours aging at 190 C.

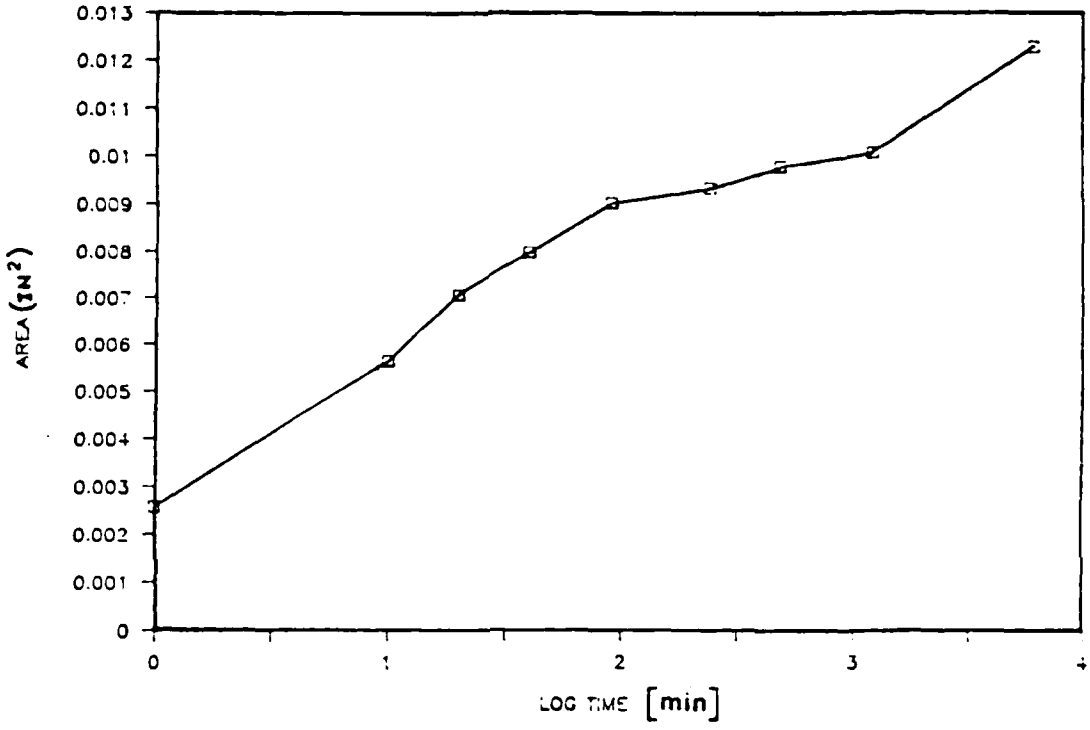

Figure 17. Relative change in volume fraction of precipitates in alloy 81 during ageing at 190 C.

after ten minutes aging at 190 C, measured from TEM micrographs was approximately 2.66 nm. The particle radius of delta prime measured from SAXS was 2.71 nm.

Figure 18 shows the Guinier radii as a function of aging time for alloy 81. From the Guinier camera and TEM results (see also Table II) it is evident that the delta prime volume fraction stays essentially constant at longer aging times. According to the coarsening kinetics, established for delta prime (73), a straight line with a slope of 1/3 is drawn through the data. The location of the points confirms that the transition from precipitation, with an increase in volume fraction, to coarsening, with a constant volume fraction, takes place around 90 minutes.

At longer aging times T1 and T2 precipitation occur. Therefore, the Ostwald line, representing the presence of one precipitate type, is no longer applicable. Figure 19 shows the increase in volume fraction of second phases with an increase in aging time at 190 C. The asterisk data points are from SAXS, the circles are data from Guinier camera analysis of the delta prime phase. The SAXS data gave a relative change in volume fraction. This data was normalized to the Guinier volume fraction at 40 minutes aging time. Beyond 90 minutes aging time the SAXS data shows an increasing volume fraction of second phases present. This is due to the presence of the T1 and T2 phases. This data confirms that the volume fraction of delta prime remains essentially constant after approximately

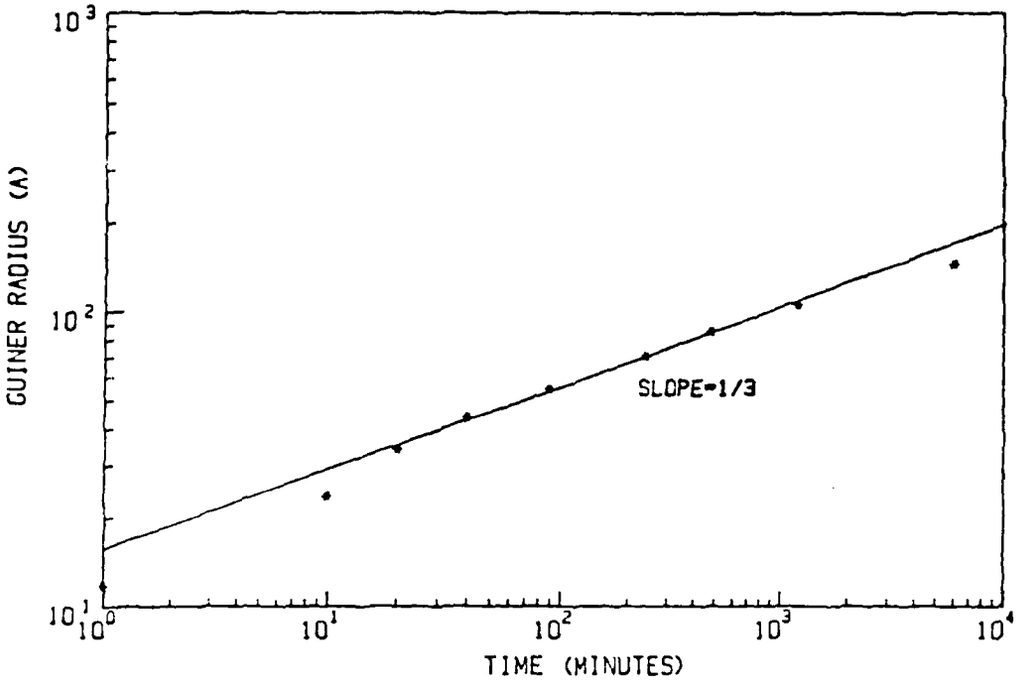

Figure 18. Guinier radius as a function of aging time at 190 C for alloy 81.

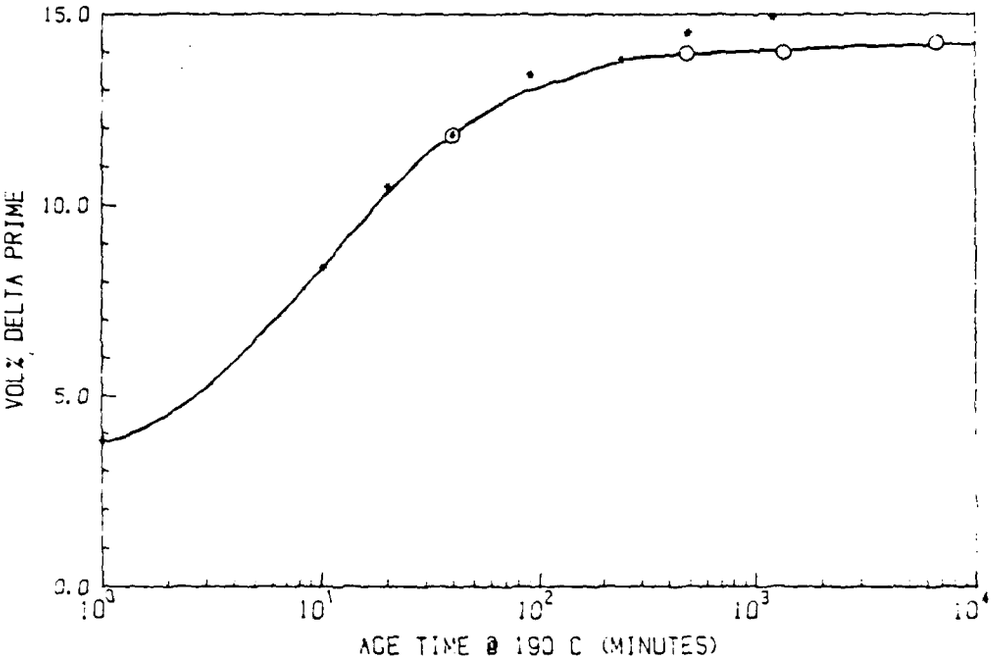

Figure 19. The volume fraction of delta prime in alloy 81 after aging at 190 C. o Guinier camera data * SAXS data normalized.

4.2 Texture

The texture of the alloys was examined in the solution heat treated condition. Texture analysis indicates that all three ternary alloys have a (110)[112] texture (See figure 20). This is a common texture present in rolled aluminum. Quantitative information is printed below each pole figure. The first number represents the average intensity normalized with respect to a random sample, from the area over which the X-ray data was collected. The second number represents the minimum intensity divided by the average intensity. The third number is the maximum intensity divided by the average intensity. The sharpness of a certain type of texture can be quantified by using these numbers.

In each direction there is a preferred orientation. There is not an extremely strong singular orientation, but most definitely one orientation is predominant. Alloys 73, 81 and 82 exhibit a strong component in the rolling direction which is a [112] direction. This indicates that the predominant orientation in the longitudinal direction is [112]. The predominant orientation in the long transverse direction is [111], and the predominant orientation in the short transverse is [110]. Although the orientation may be the same preferred orientation for each alloy, the intensity of orientation differs between samples. Alloy 82 has a stronger texture than either alloy 73 or 81.

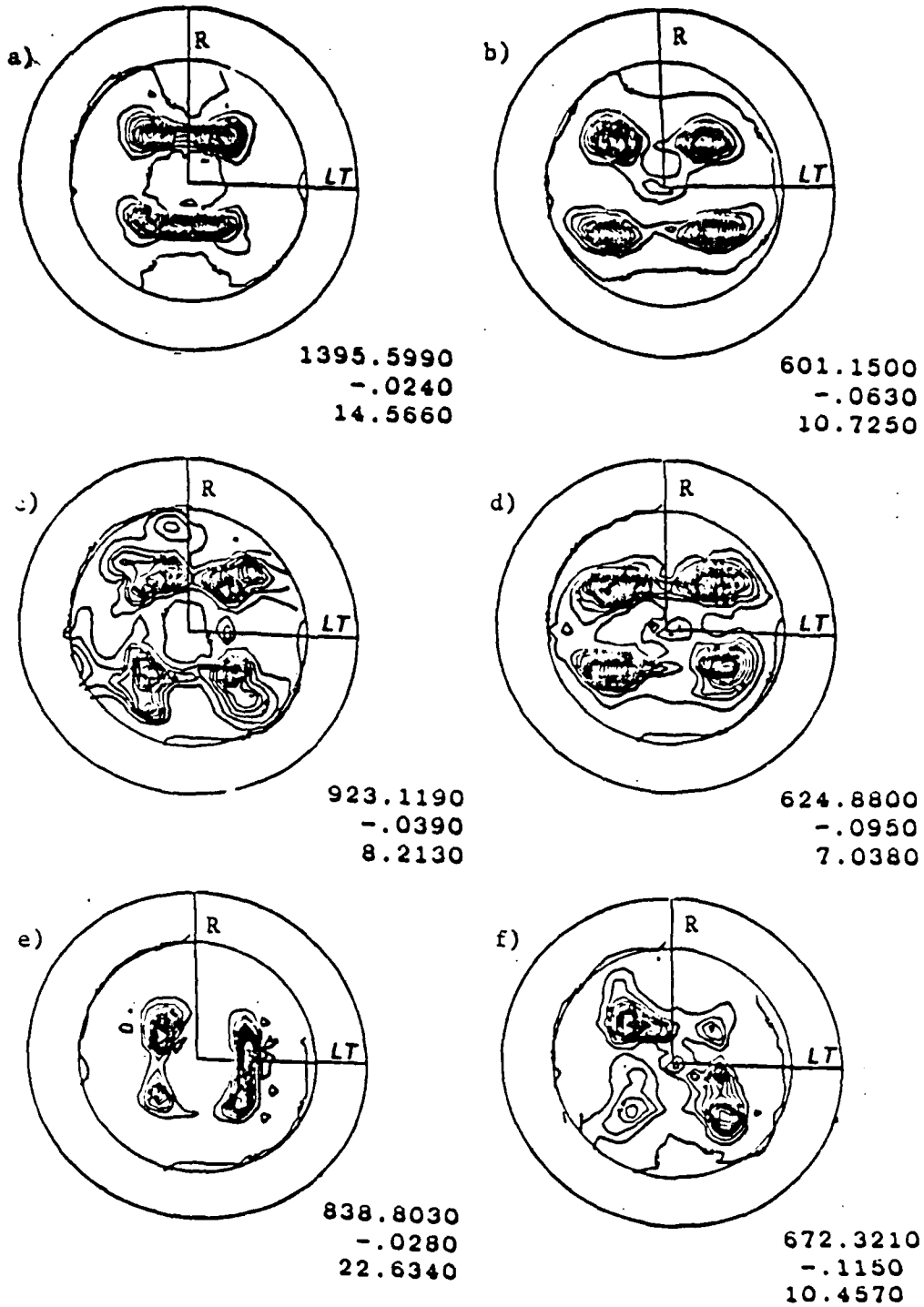

Figure 20. Pole figures a) Alloy 73 (111), b) Alloy 73 (200) Alloy 81 (111), d) Alloy 81 (200), e) Alloy 82 (111), and f) Alloy 82 (200).

4.3 Density

Experimental and calculated densities are given in Table III. The experimentally measured density values remained the same during aging for each alloy to the hundreths place. The density was calculated for our alloys using the equation given by C.J. Peel et al. (66). This equation calculates the density as the sum of the densities of the constituent elements, weighted by the atomic fractions of the respective elements. There is excellent agreement between our experimental data and the calculated values. Although the calculated equation does not include zirconium, the amount of zirconium is small and therefore, does not have a significant effect.

The experimentally measured densities did not change upon aging. Therefore, the presence of second phases did not affect the density. The nucleation and growth of delta prime did not have a significant effect on the density. The delta prime has approximately the same lattice parameter as the matrix. The presence of the T1 and T2 phases also did not show a significant effect upon our density measurements. However, there was a variation in density between the alloys. Alloy 73 has a higher density than alloy 81 or 82. Although alloy 73 has a higher lithium content, which decreases the density, it also has a higher copper content, which increases the density.

TABLE III

ALLOY	DENSITY (g/cc)	
	Experimental	Calculated
73	2.58	2.582
81	2.55	2.546
82	2.57	2.563
Binary	2.54	2.536

4.4 Pulse Echo Measurements

Transverse and longitudinal velocity measurements were recorded for all the alloys examined. The transverse velocities were approximately 3000 m/sec. The longitudinal velocities were approximately 6000 m/sec. The amount of variation between pulses was a maximum of +/- 1.6% for the transverse velocity and +/- 1.8% for the longitudinal velocity. It is observed from our data that a decrease in the transverse velocity causes a decrease in the Young's modulus, and a decrease in the longitudinal velocity causes a decrease in the Young's modulus. Similarly, a decrease in the transverse velocity causes a decrease in the shear modulus. This is consistent with analysis of the equations used, if the other variables remain constant.

The elastic modulus of the binary aluminum-lithium alloy is given in figure 21. The data points represent our the experimental data. A standard was tested under the same conditions as our experimental samples. The amount of error is about +/- .25% or 0.5 GPa for the Young's modulus measurements. The binary alloy exhibits an increase in the elastic modulus up to approximately 80 minutes aging time at 190 C. The maximum modulus observed in the binary alloy was approximately 81 GPa. 1 GPa was the largest overall change in modulus measured for the binary alloy.

The elastic modulus versus age time at 190 C for ternary alloy 81 in the unstretched condition, longitudinal direction, is given in figure 22. Our data indicate

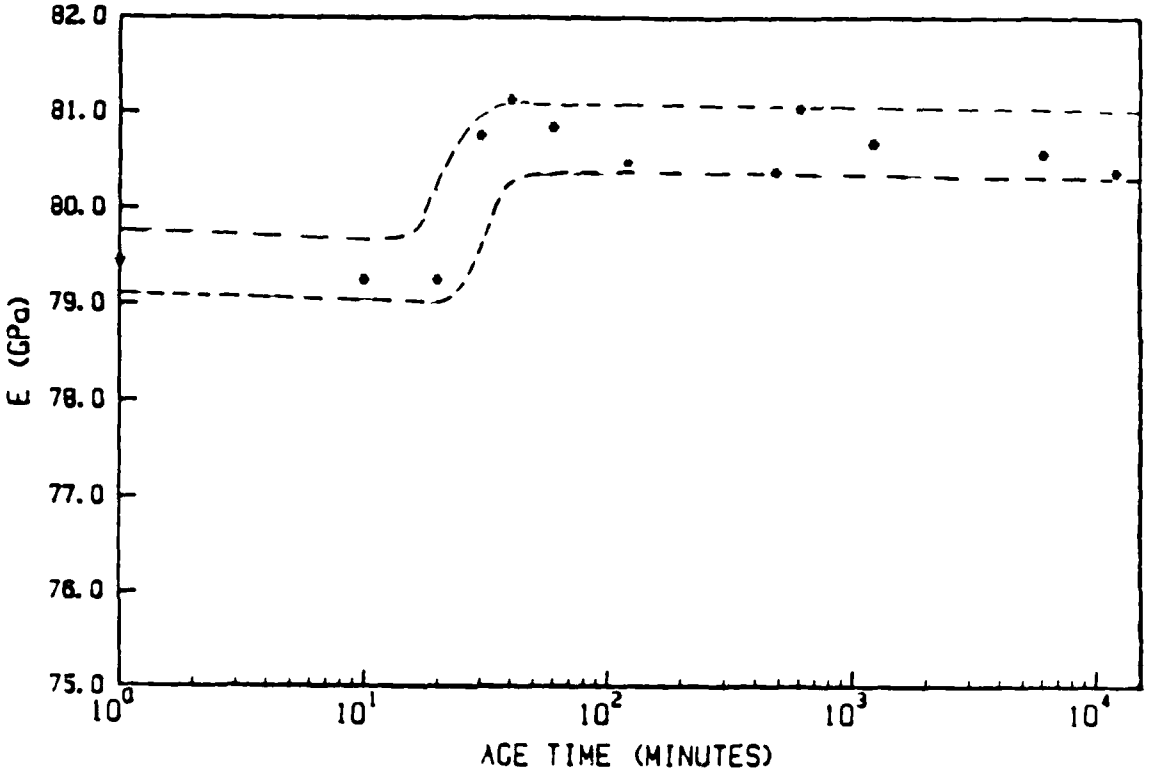

Figure 21. Elastic Modulus versus aging time at 190 C of the binary alloy

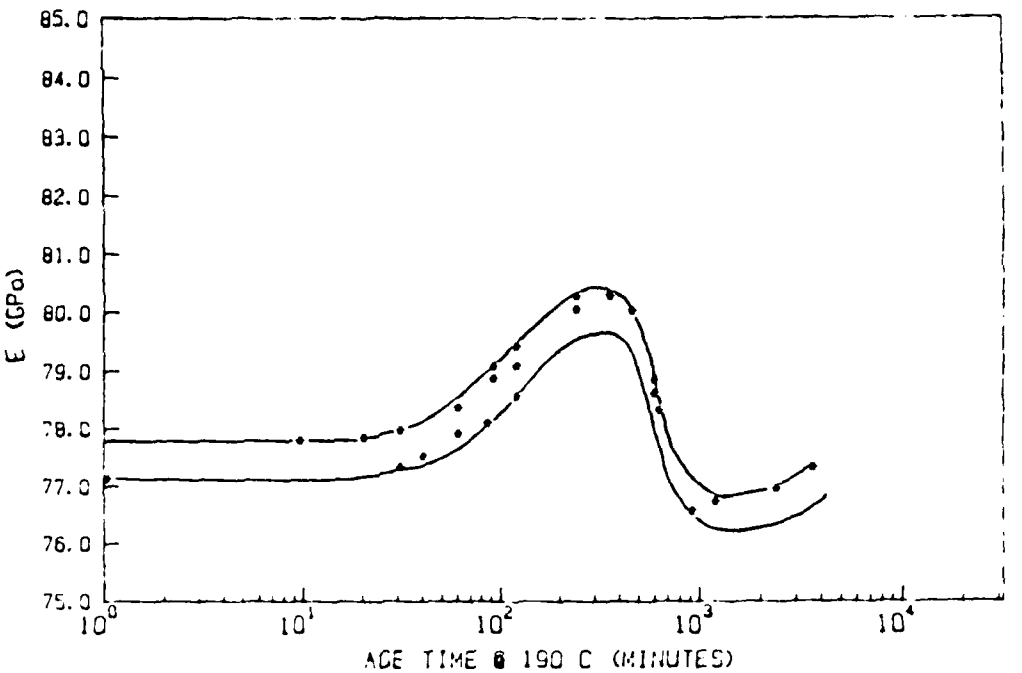

Figure 22. Elastic modulus of Alloy 81 versus aging time at 190 C. Experimental data is displayed within scatter band.

similar trends in alloys 73, 81 and 82. These are depicted in figure 23. In this figure the data points have been omitted for clarity. The elastic modulus varied as a function of aging time. The modulus values ranged from 76 to 82 GPa. Alloy 73 displayed the highest moduli for all aging times. At short aging times, up to 90 minutes, Alloy 81 exhibited a higher modulus than alloy 82. However, beyond 90 minutes their moduli were very similar. All three alloys demonstrated similar trends in the variation of modulus with aging time.

The ternary alloys reached a maximum elastic modulus at approximately 10 hours aging at 190 C. The maximum modulus for alloy 73 was 82 GPa. Alloys 81 and 82 reached a maximum of approximately 80 GPa.

The modulus of alloy 73 in the stretched condition is approximately 2 GPa lower than the unstretched material. The modulus of alloy 73, stretched 6%, versus aging time at 190 C is given in figure 24. The maximum modulus occurs almost ten hours earlier due to the faster precipitation kinetics in the stretched material.

The modulus of alloy 73, stretched 6%, which was aged at 300 C, is given in figure 25. The modulus in this alloy increases more rapidly than the unstretched condition. Although the increase is more rapid, the modulus does not reach as high a value as the unstretched material. The maximum modulus in the stretched material aged at 300 C is 78 GPa.

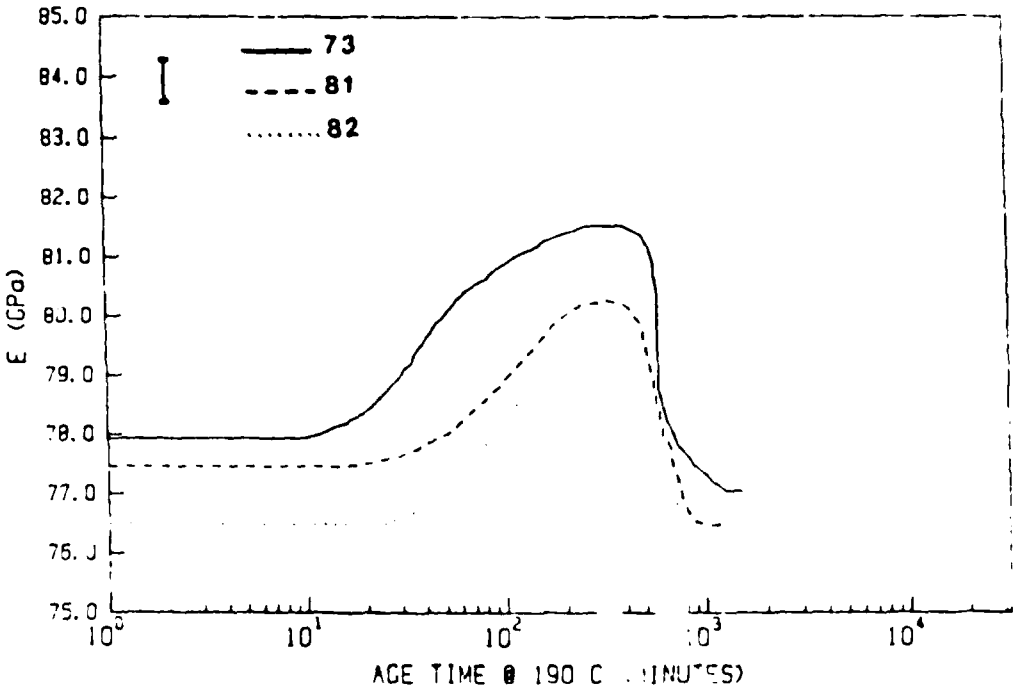

Figure 23. Young' modulus versus aging time at 190'C for alloys 73, 81 and 82 in the longitudinal testing direction.

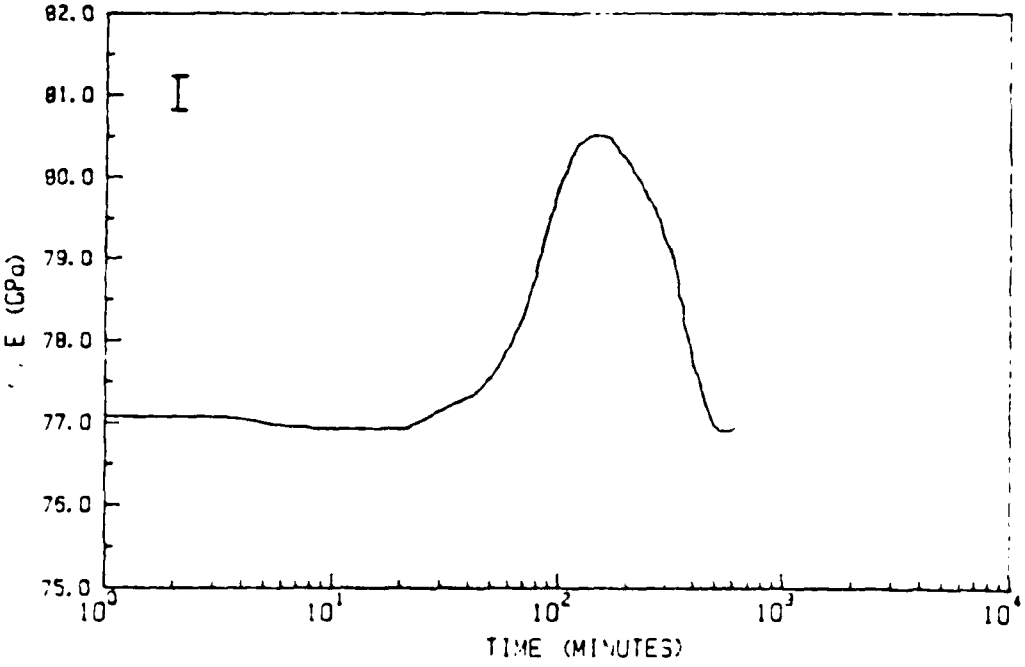

Figure 24. Young's Modulus versus aging time at 190 C of alloy 73 stretched 6%.

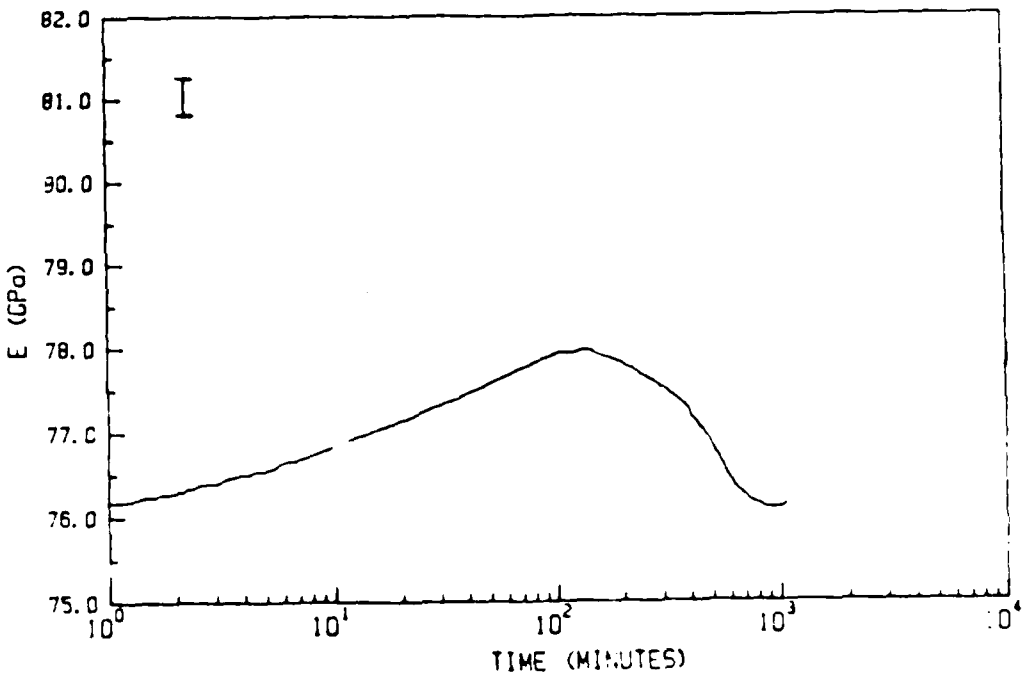

Figure 25. Young's Modulus versus aging time at 300 C of alloy 73 stretched 6%.

There is not a significant difference in the elastic modulus with regard to testing direction in all the alloys, despite the presence of a fairly pronounced rolling texture (See figure 26). It is evident that although different precipitate phases are present, they have no measurable influence on the orientation dependence of the elastic modulus. The differences between the curves in figure 26 are well within experimental error.

The shear modulus follows the same trends as the Young's modulus (see figure 27). The values range from 29 to 31 GPa. The amount of error from comparison with a standard sample is 0.2%. The shear modulus is highest for alloy 73, followed by alloy 81 and alloy 82. However, the absolute changes in shear modulus are not as large as the changes exhibited by the Young's modulus.

Poisson's Ratio Measurements as a function of aging time at 190 C are given in figure 28. There is not a significant variation in the Poisson's ratio for any of the alloys examined. All values are between 0.30 and 0.33. This is reasonable for aluminum alloys. A standard sample, alloy 7475 T651 was measured at the same time as our experimental alloys. The average Poisson's ratio for alloy 7475 T651 was 0.3397. The maximum amount of scatter measured for the Poisson's ratio of the standard was +/- .01. This is the maximum amount of error which we assume for our values.

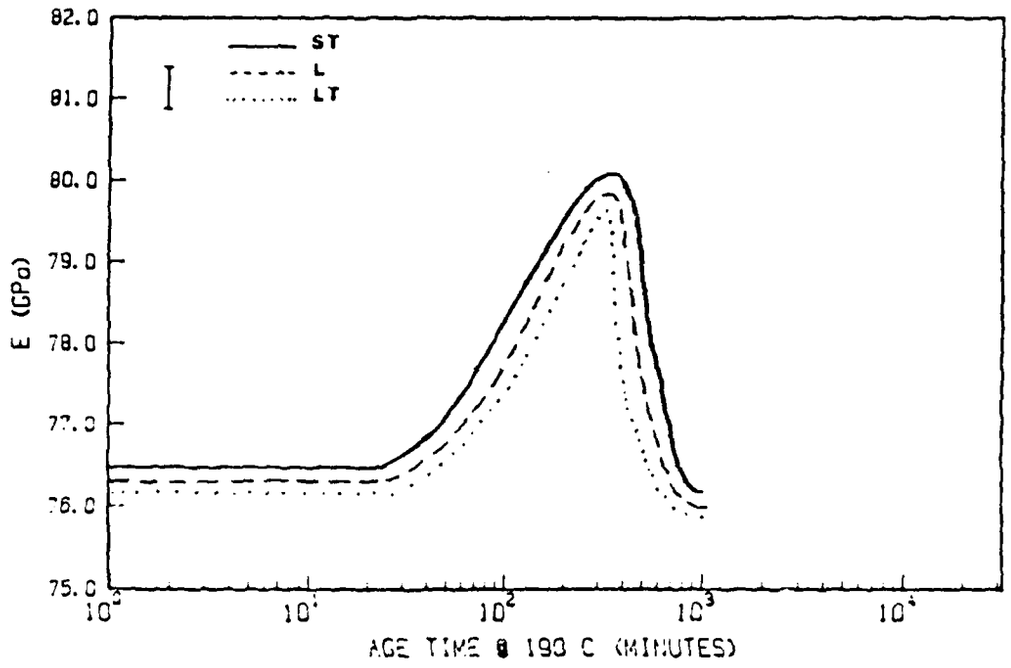

Figure 26. Young's Modulus versus aging time at 190 C for the short transverse, long transverse and longitudinal directions of alloy 82.

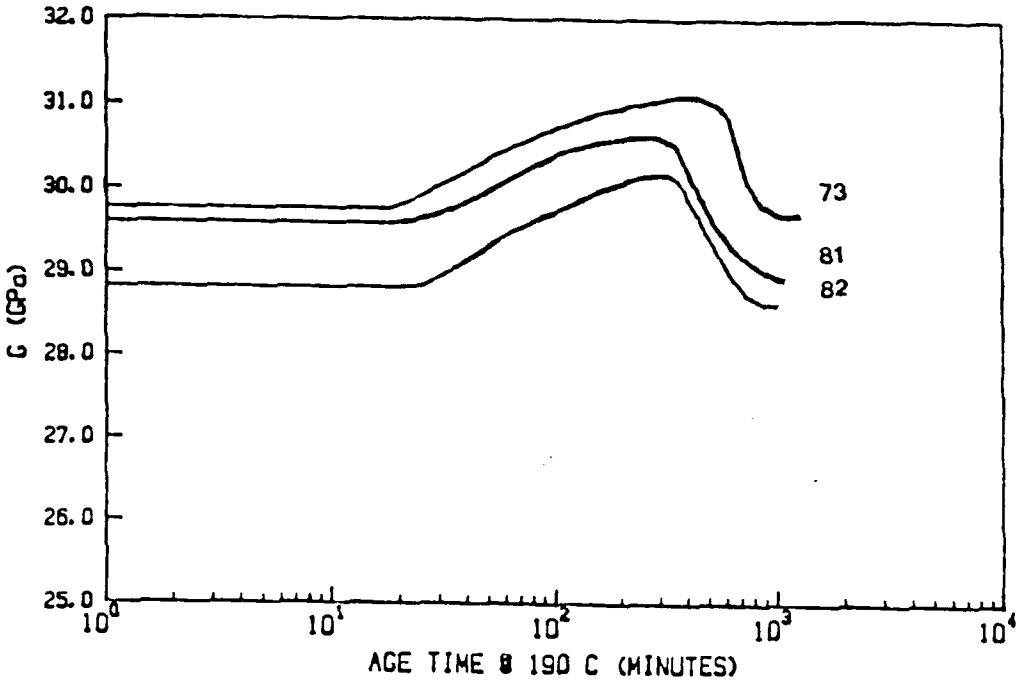

Figure 27. Shear modulus vs aging time at 190 C for alloys 73, 81 and 82.

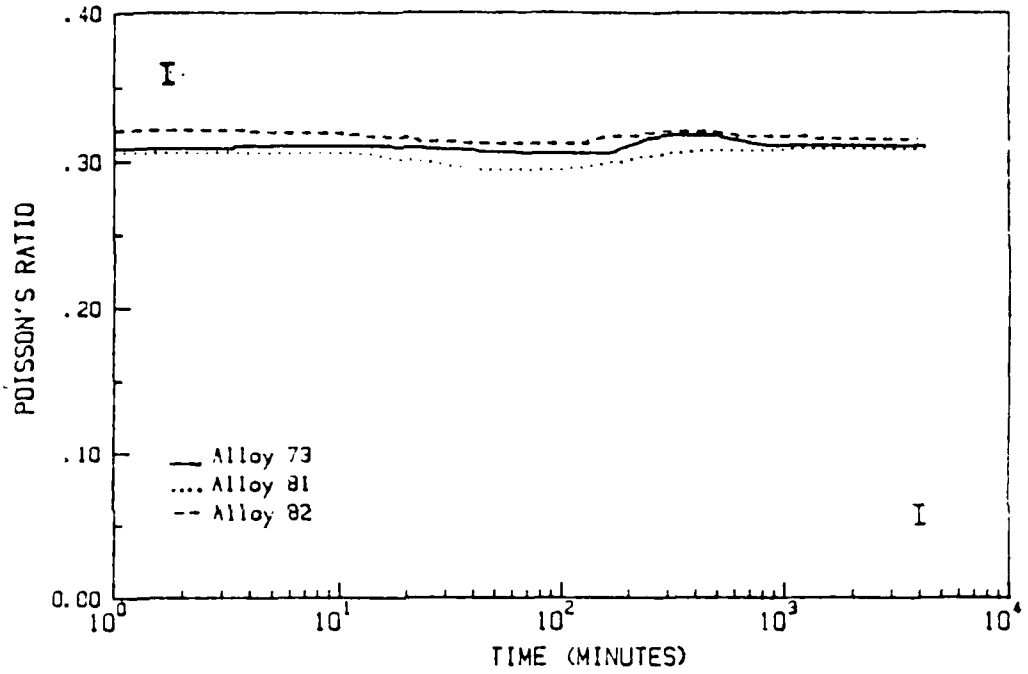

Figure 28. Poisson's Ratio versus aging time at 190 C for alloys 73, 81 and 82.

Chapter 5

DISCUSSION

The variation in elastic behavior exhibited by these alloys can be explained by changes in the microstructure. During aging, the grain size, grain orientation (texture) and density remain unchanged. Therefore, the precipitation of second phases is responsible for the changes in elastic behavior.

5.1 Binary Alloy

The Young's modulus of the binary alloy during aging at 190 C ranges from approximately 79.4 to 80.7 GPa (See figure 21, p.66). The maximum change in modulus is about 1 GPa considering the scatter band. One can safely assume that the volume fraction of delta prime stays constant after about 100 minutes of aging. According to Broussaud and Thomas (23) and Muller et al. (17) the coarsening of delta prime has only a very small effect on the Young's modulus. It is well below the accuracy of our experimental method. For these reasons the modulus does not change at longer aging times.

A volume fraction for delta prime of 11.5% was calculated using the lever rule with the miscibility gap data reported by Cocco et al. (24). This corresponds well with 12.6%, a value determined with the Guinier camera on a

binary specimen which had been aged 200 hours. The difference between the calculated and the measured value could be caused by a deviation of only 0.16 at% lithium (0.05 wt% Li) from the nominal lithium concentration in the alloy. The modulus of delta prime can be calculated by writing equation 2.2 as follows:

$$E^m = f_{\delta'} E_{\delta'}^m + (1-f_{\delta'})(E_{Al} + X\, C_{ss}^{Li})^m \qquad \text{eq. 5.1}$$

m - exponent

E - measured modulus

$f_{\delta'}$ - delta prime volume fraction

$E_{\delta'}$ - modulus of delta prime

E_{Al} - modulus of aluminum

X - constant which depicts the dependence of the modulus of the matrix phase on the amount of lithium in solid solution.

C_{ss}^{Li} - Lithium concentration in solid solution (6.25 at% at metastable equilibrium)

E_{Al} and X have been determined by a linear regression of data reported by Muller et al.(17) and Noble et al.(10). They are 70.8 and 1.253, and 69.1 and 1.764, respectively. The modulus of delta prime calculated using the above equation with E = 80.7 GPa is listed in the table below.

	Muller		Noble	
	m=1 (Voigt)	m=-1 (Reuss)	m=1 (Voigt)	m=-1 (Reuss)
E (GPa)	96.6 +/-1.7	101.0 +/-2.5	85.4 +/-2	85.8 +/-2.3

The values determined from Muller's data are close to 106 and 96 GPa reported elsewhere (10,17,23). Using the analysis from Muller's data, the modulus of the matrix phase is dependent on the amount of lithium in solid solution to a lesser extent than Noble's data. Because a stronger dependence follows from Noble's data, the contribution of delta prime to the modulus is smaller. The reason for the different relationships between the modulus of the solid solution and its lithium concentration lies in the experiments done by Muller et al. and Noble et al. The former used single crystals of different lithium concentrations and calculated the polycrystalline moduli for a texture free specimen. The latter used polycrystalline specimens which have been extruded and rolled into thin strips. In this case variations in modulus may occur not only due to different lithium concentrations but also due to differences in crystallographic texture and stored energy due to working from alloy to alloy.

Equation 5.1 can also be used to predict the change in modulus as a function of the volume fraction of delta prime. The change in lithium concentration in the solid solution

(C_{ss}^{Li}) can be shown to be related to the delta prime volume fraction according to equation 5.2.

$$C_{ss}^{Li} = (Y^{Li} - C^{Li}_{\delta'} f_{\delta'}) / (1 - f_{\delta'}) \qquad \text{eq. 5.2}$$

Y^{Li} is the total atomic fraction of lithium in the alloy and $C^{Li}_{\delta'} = 0.225$ according to Cocco et al. (24).

Figure 29 shows the calculated overall modulus of the binary alloy as a function of delta prime volume fraction according to equations 5.1 and 5.2. As in the previous calculations, parameters derived from single crystal (17) and polycrystalline (10) work have been used. It is evident from this figure that the single crystal results from Muller et al. are more realistic. They predict, depending on the averaging method, a modulus increase with an increasing volume fraction of delta prime. The linear rule of mixtures, i.e. Voigt averaging, predicts an increase of approximately 1 GPa from 0 to 11.5 vol% delta prime. This fits well with the experimentally measured increase in modulus. Assuming the same stress in all phases, i.e. Reuss averaging, predicts essentially no change in modulus with aging. This is definitely not seen in the present results and contradicts results from other researchers (23). The strain transfer between matrix and second phase with coherent precipitates is believed to be complete and the linear rule of mixtures is applicable (21).

The curves calculated from analysis of data from Noble

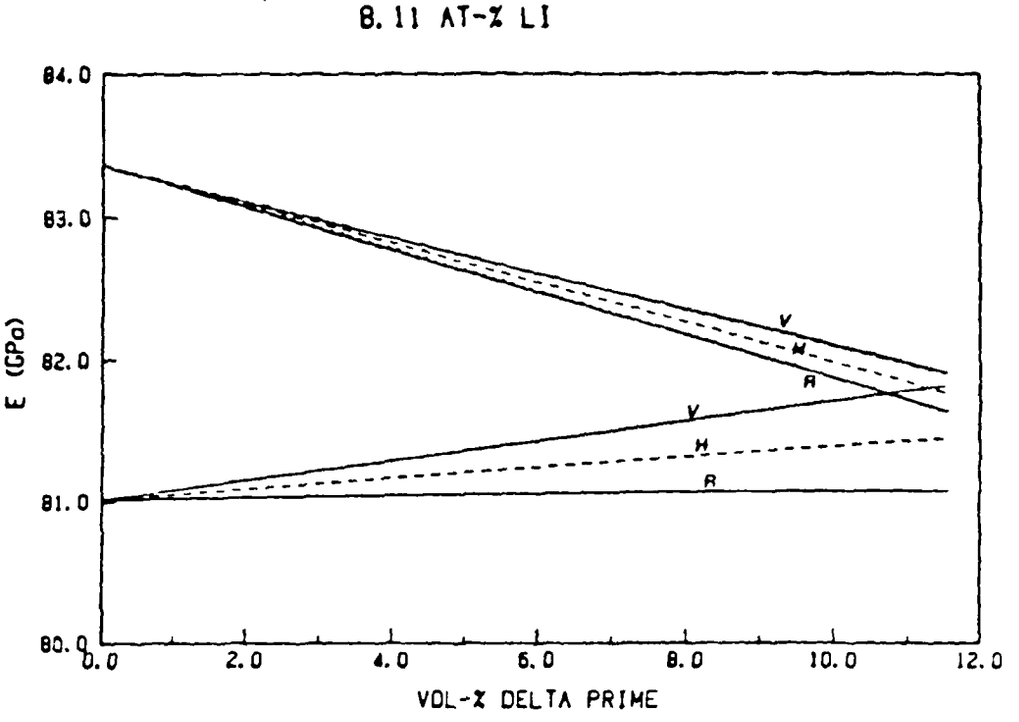

Figure 29. Elastic modulus versus volume fraction delta prime. Voigt and Reuss averaging techniques are compared. Hill represents the arithmetic average of Voigt and Reuss. Curves have been calculated using data from Muller et al.(17) and Noble et al.(10).

et al. show a continuous, unrealistic drop in modulus with precipitation.

The change in modulus in figure 21, p.66, with aging time is due to the kinetics of the delta prime precipitation process. This point will be addressed in more detail in the discussion of the ternary alloys.

5.2 Ternary Alloys

The modulus values differed in magnitude for each ternary alloy. This may be due to differences in the composition. An attempt can be made to calculate the modulus for the as solution heat treated condition, assuming all the elements are in solid solution:

$$E = E_{Al} + X_{Li}\, C_{Li} + X_{Cu}\, C_{Cu} \qquad \text{eq. 5.3}$$

E_{Al} = 70.8 GPa

X_{Li} = 1.253 (17)

X_{Cu} = 2.0 (67)

C = concentration of elements in at%

The results from equation 5.3 are listed in the table below:

ALLOYS

	73	81	82	Method
E (GPa)	83.8	83.0	81.7	eq. 5.3
E (GPa)	77.9	77.5	76.2	measured

Although the calculated values for the moduli are higher than the ones measured, the trend and the differences between the alloys are confirmed. However, one has to keep in mind that this simple calculation neglects the influence of texture and the fact that some delta prime precipitation has already taken place (See figure 8, p.43).

Up to approximately 90 minutes aging the unstretched ternary alloys can be treated as two phase materials comprised of the solid solution and delta prime phases. In the early stages of aging the nucleation of T1 is hindered. For an alloy containing precipitates in the as quenched condition, the aging kinetics can be described by equation 5.4 from D. Turnbull (70).

$$f_{\delta'} = f_{\infty} \left(1 - \left(1 + B\,(t+t_0)\right)^{-1/3}\right) \qquad \text{eq. 5.4}$$

f_{∞} - equilibrium volume fraction
$f_{\delta'}$ - volume fraction of delta prime at time, t
t_0 - constant
B - constant

Figure 30, p.84, shows that equation 5.4 describes well the measured change in volume fraction of delta prime up to about 100 minutes age time. The parameters used were f_{∞} =0.2, t_0 = 2.7705 minutes and B = 0.3196 minutes^{-1}. At longer aging times the number of phases increases to three and the conditions for which the equation has been derived do not prevail any more. It is interesting to note that the equilibrium delta prime volume fraction for a binary alloy having the same lithium concentration as alloy 81 is 17%

from the phase diagram. This value is not reached in the ternary alloy due to the precipitation of T1 and T2.

The combination of equations 5.1, 5.2 and 5.4 allows the calculation of the change in modulus in alloy 81 with aging time up to the point where T1 begins to precipitate. The constants in equation 5.1 were derived from data from Muller et al. (17). It has been shown in section 5.1 that their single crystal work provides an adequate description of the results from the binary alloy. Figure 31, p.85, shows that the modulus calculated this way and the measured curve for alloy 81 compare well. An additive correction of - 5.5 GPa has been made to the theoretical curve in order to compensate for offset. This correction had to be made in order to correct for points such as the following:

- the calculation is based upon single crystals which have a low dislocation density,
- the theoretical values are for a texture free material,
- the "machine constant" of the pulse echo equipment is unknown.

The increase in E after about 90 minutes is caused by T1 precipitation. This confirms earlier work (27) which has shown a beneficial effect of T1 on the modulus in Al-Li-Cu-Mg alloys. T1 volume fraction measurements below 5 hours were not possible due to weak T1 diffraction lines in the Guinier camera. Therefore, an analysis involving the T1

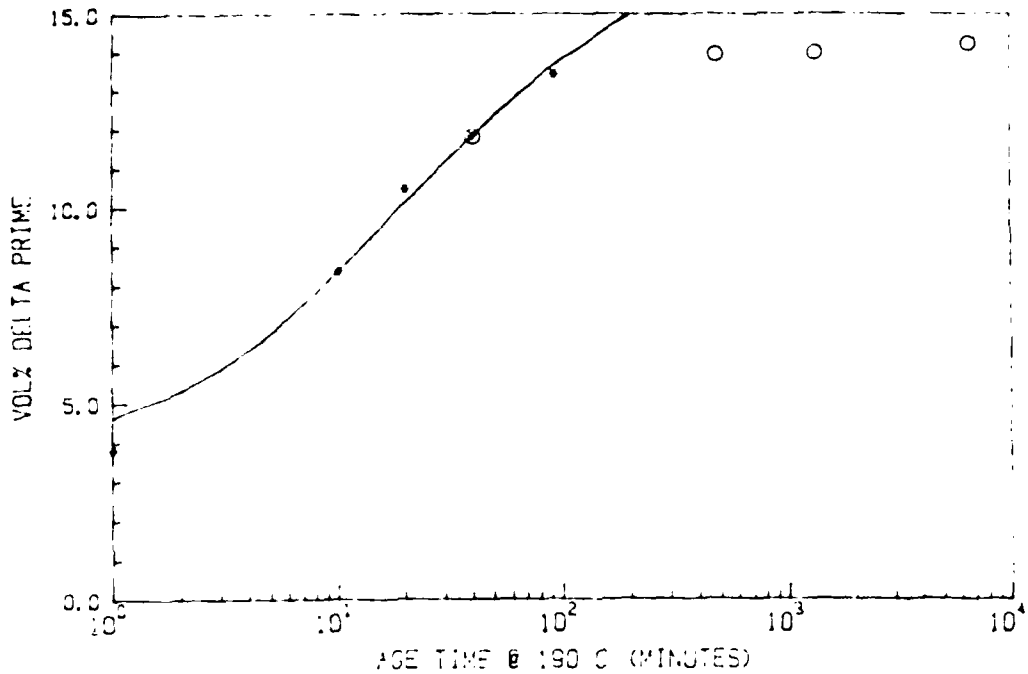

Figure 30. Change in volume fraction of delta prime with aging time at 190 C. Solid line represents theoretical prediction by D. Turnbull (70), asterisk represents SAXS data, and open circles represent Guinier camera data.

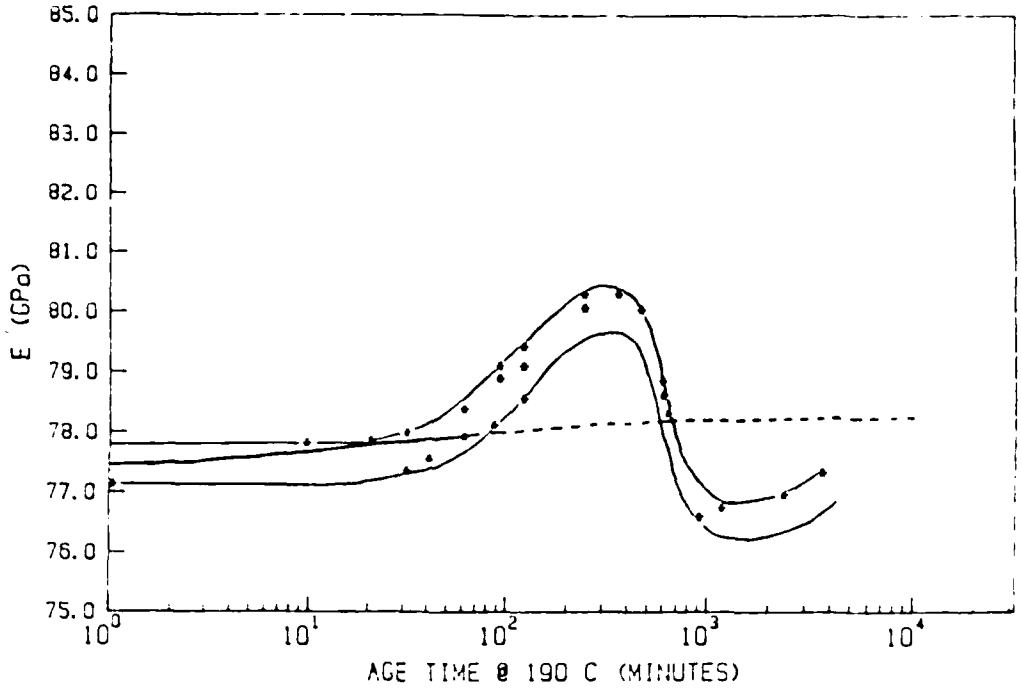

Figure 31. Elastic modulus versus aging time for alloy 81. Experimental data is compared with a theoretical prediction.

precipitation kinetics similar to the one carried out for delta prime could not be done. However, a T1 volume fraction was obtained from Guinier camera analysis at 8 hours where the T2 phase is still absent. The intensities of a T1 (002) diffraction peak and an aluminum (111) diffraction peak were calculated and compared. In these calculations a T1 structure as proposed by Huang and Ardell (71) has been used to determine the structure factor. Anomalous dispersion correction has been done according to (72). A volume fraction of 0.07 T1 was calculated. Knowing the volume fraction of T1 equation 2.2 can be rewritten as the following:

$$E_{T1} = (E_{measured} - (f_{\delta'} E_{\delta'} + f_{ss} E_{ss}))/ f_{T1} \quad \text{eq. 5.5}$$

This equation is for a linear rule of mixtures. By using equation 5.3 for the modulus of the solid solution a modulus of 350 GPa results for T1. It is interesting to note that the solid solution of alloy 81 at this point contains calculated values of 0.6 at% lithium and .035 at% copper. The accuracy of the value in the present work is about +/- 15 GPa (+/- 5%) if one considers the scatterband. A similar calculation for the Reuss rule of mixtures results in a negative modulus. This result indicates that the Reuss type of averaging is not applicable to T1. The real intrinsic modulus of T1 can only be measured on a sample which is 100% T1. In this research, several attempts

have been made to measure the modulus of an almost 100% T1 specimen, but due to internal cracks in the material experimental difficulties arose.

The drop in modulus occurs at approximately 8 to 10 hours aging time with the precipitation of the icosahedral T2 phase. Its structure is not completely understood. Therefore, the volume fraction calculations which were performed for other phases could not be done. The data suggest that T2 has an extremely low intrinsic modulus because its volume fraction appears to be fairly small. From figure 19, p.60, it follows that the volume fraction of delta prime at these aging times stays more or less constant. This indicates that the T2 phase may grow at the expense of the T1 phase but not at the expense of delta prime. It may also take Li out of solid solution, thus decreasing the modulus of the matrix phase even further.

The increase in E at very long aging times is expected to be caused by precipitation of equilibrium phases. Guinier analysis indicates, in addition to the delta prime, T1, T2 and matrix phases, there is delta phase present after 100 and 300 hours aging time at 190 C. The delta phase has an intrinsically high modulus. Its reported value ranges from 105 GPa (10) to 90 GPa (3).

Although the type of precipitates in all three ternary alloys are the same, their kinetics are different. The earlier onset of T1 precipitation in the high copper alloy

AD-A182 154 INVESTIGATION OF THE ELASTIC BEHAVIOR OF AL-LI-X ALLOYS 2/2
(U) VIRGINIA UNIV CHARLOTTESVILLE DEPT OF MATERIALS
SCIENCE W W RUCH ET AL 01 JUN 87 UVA/525400/MS87/102
UNCLASSIFIED N00014-85-K-0526 F/G 11/6 1 NL

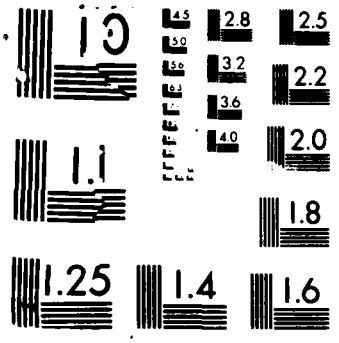
1.0
1.1
1.25
1.4
1.6
1.8
2.0
2.2
2.5
2.8
3.2
3.6
4.0
4.5
5.0

73 shows up as an earlier increase in modulus (see figure 23, p.69) and a larger difference between starting and peak modulus condition. The latter may be explained by a higher T1 volume fraction.

The modulus of alloy 73 in the stretched condition is approximately 2 GPa lower than the unstretched material. This is due to the increased amount of dislocations and point defects in the stretched material. The increased amount of dislocations allows for a more homogeneous precipitation of the T1 phase within the matrix as opposed to along the grain boundaries. The dislocations provide sites which contribute energy to overcome the activation barrier necessary for nucleation. The increased amount of point defects also allows for an increased rate of diffusion. This contributes to increasing the amount of precipitation. The modulus increase in the stretched material occurs at shorter age times than the unstretched. This is due to the increase in the kinetics of precipitation.

The modulus of alloy 73, stretched 6%, which was aged at the higher temperature, increases more rapidly due to faster diffusion rates. The modulus increases more rapidly, but does not reach as high a modulus as the unstretched material. The maximum modulus in the stretched material aged at 300 C is 78 GPa. This relatively low value is due to the absence of delta prime and the fact that T2 forms earlier at these high temperatures. At 300 C the formation of delta prime is surpressed because one is above the delta

prime solvus temperature.

5.3 Directionality

The texture of the solution heat treated condition was examined. Work done by Bull and Lloyd demonstrates that thermal treatments such as solution heat treatments do not substantially alter the texture obtained from rolling in aluminum-lithium alloys (68).

There may be a significant difference in the elastic modulus for different crystallographic orientations (28). Relationships for elastic constants of aluminum-lithium solid solution alloys have been determined by Muller et al.(17) Linear regression analysis was performed on Gerold's experimental data to determine the elastic constants for our alloys. The values for C_1 had a R^2 value of 0.384. The R^2 for the regression analysis of C was 0.988. The R^2 value for C' was 0.995. The Elastic constants for alloy 81 was calculated from C_1, C and C'. Using these elastic constant values the elastic modulus was calculated (75) and is listed in Table IV along with pure aluminum from reference (12).

The highest moduli were found to be in the [111] direction; this is expected. One can see from Table IV that the maximum theoretical difference in E due to orientation effects (ΔE_{max}) is only about half in aluminum-lithium alloys compared to pure aluminum. However, the moduli which were calculated for the [112] direction were

higher than our experimental values in the longitudinal direction. There are several reasons for this. Firstly, the alloys are polycrystalline. Hence, they do not exhibit a single orientation. Secondly, the alloys examined are ternary alloys, not binary aluminum-lithium. The presence of other alloying additions will have different effects on the elastic constants. Thirdly, not all the lithium is in solid solution.

It is expected that the highest moduli will be found in the long transverse direction, which has an above random share of [111] directions. However, the differences in E with testing direction are within our experimental scatterband (see figure 26, p.73) for all aging times.

Table IV

Theoretical moduli for solid solutions

Alloy	Crystallographic Direction (hkl)				
	111 (LT)	110 (ST)	100	112 (L)	ΔEmax (%)
82	83.60	81.38	75.38	81.38	11%
Al	75.30	71.73	62.81	71.73	20%

This fact indicates that the second phases such as delta prime, T1 and T2 do not have a strong intrinsic orientation dependence which effects the overall modulus. It has been shown by Muller (74) that the spherical delta prime phase is isotropic. Our data support this conclusion.

Chapter 6

CONCLUSIONS

1) The Young's modulus increases only slightly due to delta prime precipitation (0.08 GPa/vol%).

2) The T1 phase contributes positively to the elastic modulus. Its intrinsic modulus is estimated to be 290 GPa using a Voigt linear rule of mixtures.

3) A maximum increase in E with aging time of about 5% can be attributed to delta prime and T1 precipitation for the alloys examined.

4) There is a significant drop in modulus (up to 5%) at peak age. It is associated with T2 precipitation, which occurs at the expense of T1 but not at the expense of delta prime. T2 formation also possibly depletes the solid solution concentration of lithium. These effects, combined with a low intrinsic modulus of T2, may explain the pronounced decrease in E.

5) Stretched Al-Cu-Li alloys will show a smaller , but faster modulus increase with aging when compared with unstretched counterparts. Earlier occurrence of T1 and enhanced precipitation kinetics are responsible for this phenomenon.

6) In order to have an Al-Cu-Li alloy with maximum modulus the T2 phase has to be avoided.

7) There is no orientation dependence of the elastic modulus observed in these alloys.

REFERENCES

1. E.A. Starke Jr., T.H. Sanders Jr.,and I.Palmer, "New Approaches to Alloy Development in the Al-Li System", Journal of Metals, 33 (1981) p.24

2. G.G. Wald, NASA Contractor Report 16576, Lockheed - California Company, Burbank CA, May (1981)

3. W. Koster and W. Rauscher, Z.Metallkde, 39 (1948) p.111

4. K.K. Sankaran and N.J. Grant : Aluminum-Lithium Alloys, ed. by T.H. Sanders Jr. and E.A. Starke Jr., TMS-AIME, Warrendale PA, (1981) p.205

5. T.H. Sanders Jr. and E.S. Balmuth, Metals Progress, 113 (1978) p.32

6. I.F. Sakata, "Systems study of Transport Aircraft Incorporating Advanced Aluminum Alloys - Final Report", NASA CR-165820, NASA Contract NAS 1-16434, Jan. (1982)

7. W.E. Quist, G.H. Narayanan and A.L. Wingert, "Aluminum - Lithium Alloys for Aircraft Structures - An Overview", Aluminum-Lithium Alloys II, ed. T.H Sanders Jr. and E.A. Starke Jr., TMS-AIME, Warrendale PA, (1983) p.313

8. H.J. Axon and W. Hume-Rothery, Proc. Roy. Soc., London, Vol. 193A, (1948) pp. 1-24

9. R.S. Leigh, "A Calculation of the Elastic Constants of Aluminum", Phil. Mag, Vol.7, 42 (1951) p.139

10. B.Noble and S.J. Harris and K.Dinsdale, "The Elastic Modulus of Aluminum-Lithium alloys", Journal of Materials Science, 17 (1982) p.461-468

11. R.W. Hertzberg, Deformation and Fracture Mechanics of Engineering Materials, John Wiley and Sons Inc., New York N.Y. (1976) p.6

12. C. Kittel, Introduction to Solid State Physics, 4th Edition, John Wiley and Sons Inc., New York N.Y. (1971) p.149

13. J.R. Neighbors, "An Approximation Method for the Determination of the Elastic Constants of Single Crystals", Journal of Acoustical Society of America,

26, Sept.(1954) p.865

14. D.Gerlich, Physical Review A, vol.135 (1964) p.1331

15. N.J. Trappeniers, S.N. Biswas, P. Van't Klooster and G.A. ten seldim, Physica 85B33 (1977)

16. H. Jones, Physica B, vol.15, (1949)

17. W. Muller, E. Bubeck and V. Gerold, "Elastic Constants of Al-Li solid solutions and precipitates", Aluminum-Lithium Alloys III, Institute of Metals, London (1986) p.435

18. W.Voigt, Lehrbuch der Kristallphysik, B.G. Teubner, Verlag, Stuttgart (1966)

19. A.Reuss,"Berechnung der Fliessgrenze von Mischkristallen auf Grund der Plastizitatsbedingung fur Einkristalle", Z. angew. Math. Mech., 9 (1929) p.49

20. R.Hill, "The Elastic Behavior of a Crystalline Aggregate", Proc. Phys. Soc., A65 (1952), p.349

21. M.E. Fine, "Elastic Moduli of Two Phase Aluminum Alloys", Scripta Metallurgica vol.15 (1981) pp.523-524

22. J.P. Lyle, Jr., Aluminum, ed. by K.R. Horn, ASM Metals Park, Ohio (1967) Vol.I Ch.10, pp.337-358

23. F. Broussaud & M. Thomas, "Influence of delta prime on phase coalescence on Young's Modulus in an Al-2.5 wt% Li alloy", Aluminum-Lithium Alloys III, ed. by C. Baker, P.J. Gregson, S.J. Harris and C.J.Peel, Institute of Metals, London (1986) p.442

24. G.Cocco, G. Fagherazzi and L. Schiffini, "Determination of the delta prime Coherent Miscibility Gap in the Al-Li System by Small-Angle X-ray Scattering", J. Appl. Cryst., 10 (1977) pp.325-327

25. L.F. Mondolfo, Aluminum Alloys Structure & Properties, Butterworths, London-Boston (1976) p.704

26. F. Fouquet, P. Merle, M. Kohen, J. Merlin and P.F. Gobin, "Variation Du Module D'Young Associee A La Precipitation De La Phase Dans Un Alliage Al-Cu 4%", Acta Metallurgica, Vol.27 (1979) pp.315-326

27. E. Agyekum, W. Ruch, E.A. Starke Jr., S.C. Jha and T.H.

Sanders, "The Effect of Precipitate type on the Elastic Properties of Al-Li-Cu and Al-Li-Cu-Mg Alloys", Aluminum-Lithium Alloys III, Institute of Metals, London (1986) p.448

28. Hans-Joachim Bunge, "Technological Applications of Texture Analysis" Bd. 76 (1985) H.7, Z. Metallkde p.457

29. H.B Huntington, "Ultrasonic Measurements on Single Crystals", Physical Review Vol.72, No.4, Aug 15 (1947) p.321

30. Alex Vary, "Quantitative Ultrasonic Evaluation of Mechanical Properties of Engineering Materials", National Bureau of Standards Special Publication 596, Ultrasonic Materials Characterization H. Berger and M. Lomqwe eds., Proceedings of the First International Symposium on Ultrasonic Materials Characterization held at NBS, Gaithersburg MD, June 7-9, 1978 Issued Nov. 1980, p.41

31. H.B. Huntington, "The Elastic Constants of Crystals", Solid State Pysics, Vol.7, (1958) p.213-349

32. G.V. Blessing, W.L Elban and J.V. Foltz, "Ultrasonic Characterization of Aluminum Matrix Composites: Experiment and Theory", Naval Surface Weapons Center, Report NSWC/WOL TR 78-159

33. J.Krautkramer and H. Krautkramer, Ultrasonic Testing of Materials, 2nd ed., Springer-Verlag, New York, (1977)

34. I. Malecki, "Application of Ultrasonic Physics in Material Technology", Archives of Acoustics, 2, 3 (1977)

35. J.E. Zimmer and J.R. Cost, "Determination of the Elastic Constants of a Unidirectional Fiber Composite Using Ultrasonic Velocity Measurements" Journal of the Acoustical Society of America, Vol.47 No.3 (Part 2), (1970) p.795

36. M. Thomas, G. Lapasset and R.W. Cahn, Mem. Sci. Rev. Met. 9 (1984) p.438

37. J.M. Silcock, "The Structural Aging Charateristics of Aluminum-Copper-Lithium Alloys", Journal of the Institute of Metals, Vol.88 (1959-60) p.357

38. "Critically Evaluated Aluminum Phase Diagrams", Bulletin of alloy phase diagrams, American Society for Metals,

Metals Park, Ohio, Vol.3 No.2 (1982)

39. B. Noble and G. Thompson, "Precipitation Characteristics of Aluminum-Lithium Alloys", Metal Science Journal Vol.5 (1971) p.114

40. D.B. Williams and J.W. Edington, "The Precipitation of (Al_3Li) in Dilute Al-Li Alloys", Metal Science, Vol.9 (1975) p.529

41. R.Nozato and G. Nakai, Trans. JIM, 18 (1977) pp.679-680

42. J.M. Papazian, C. Sigli, J.M. Sanchez, "New Evidence for GP zones in Binary Al-Li Alloys", Scripta Metallurgica, Vol.20 (1986) pp.201-206

43. S. Spooner, D.B Williams & C.M. Sung, "Combined small angle x-ray scattering and transmission electron microscopy studies of Al-Li alloys", Aluminum-Lithium Alloys III, Institute of Metals, London (1986) p.329

44. P. Sainfort and P. Guyot, "Fundamental Aspects of Hardening in Al-Li and Al-Cu-Li Alloys", Aluminum -Lithium Alloys III, Institute of Metals, London (1986) p.420

45. B.Noble and G.E. Thompson: Metal Sci. Journal, 5, (1970) p.14

46. E. Balmuth, Scripta Met., 18 (1984) pp.301-304

47. T.H. Sanders Jr., Material Science and Engineering, 43 (1980) pp.249-250

48. G.W. Lorimer: "Precipitation in Aluminum Alloys", Precipitation Processes in Solids, Proceedings TMS-AIME, (1984) p.6

49. A.K. Hardy and J.M. Silcock: Journ. Inst. Metals, 34 (1955-56) p.423

50. H.K. Hardy, Journal Inst. Metal, Vol.84 (1955-56) p.429

51. P. Sainfort and P. Guyot, Aluminum-Lithium Alloys III, ed. by C.J. Peel, P.J. Gregson, S.J Harris and C. Baker, Institute of Metals, London (1986) p.425

52. N. Ryum, Acta Metall., Vol.17 (1969) p.269

53. W.L. Fink and Dana W. Smith, "Age Hardening of Aluminum

Alloys. IV.- Discussion of the Theory", Metals Technology, (1939), 6, (4); A.I.M.M.E. Tech. Publ. No. 1083

54. B.P. Gu, K. Mahalingam, G.L. Liedl and T.H. Sanders, "The (Al_3Li) particle size distribution in a variety of Al-Li alloys", Aluminum-Lithium III, ed. by C.J. Peel, P.J. Gregson, S.J. Harris and C. Baker, Institute of Metals, London (1986) p.360

55. W. Stimpson, M.H. Tosten, P.R. Howell and D.B. Williams, Aluminum-Lithium Alloys III, ed. by C. Baker, P.J. Gregson, S.J. Harris and C.J. Peel, Institute of Metals, London (1986) p.386

56. P. Makin and B. Ralph, J.Mat.Sci, Vol.19 (1984) p.3835

57. F.W. Gayle and J.B. VanderSande, Scripta Metallurgica, Vol.18, (1984) pp.473-478

58. T. Malis, "Characterization of Lithium Distribution in Aluminum Alloys", Aluminum-Lithium Alloys III, Institute of Metals, London (1986) pp.353

59. Landolt-Bornstein, Physikalish - Chemische Tabellen, vol.6, Springer-Verlag , Berlin (1960) p.199

60. W.A. Cassada, "Effect of Germanium on the properties of Al-2Li", Masters thesis, University of Virginia, Jan. (1985)

61. W.A. Cassada, G.J. Shiflet and S.J. Poon, "Formation of an Icosahedral Phase by Solid-State Reaction", Physical Review Letters, Vol.56, No.21 (1986) p.2276

62. D.B.Williams, Practical Analytical Electron Microscopy in Material Science, Philips Electronic Instruments Inc. Electron Optics Publishing Group, (1984) p.78

63. J.Glazer et. al. "Theoretical Analysis of Aging Response of Al-Li alloys strengthened by Al3Li Precipitates", Aluminum-Lithium Alloys III, Institute of Metals, London (1986) p.369

64. E.E. Underwood, Quantitative Stereology, Addison-Wesley, Philippines (1970) p.178

65. H.P. Klug and L.E. Alexander, X-ray Diffaction Procedures, John Wiley & Sons, New York (1954) p.410

66. C.J. Peel, B. Evans, C.A. Baker, D.A. Bennett, P.J. Gregson and H. M. Flower, "The Development and Application of Improved Aluminum - Lithium Alloys", Conference Proceedings Al-Li II, Met. Soc. AIME, Warrendale PA (1983) p.363

67. H.W. Wawra, Aluminium, 40 12 (1971) pp. 805-811.

68. M.J. Bull and D.J. Lloyd, "Textures developed in Al-Li-Cu-Mg alloy", Aluminum-Lithium Alloys III, Institute of Metals, London (1986) p.402

69. S. Ceresara, G. Cocco, G. Fagherazzi and L. Schiffini, Phil. Mag, 35 (1977) pp. 373-378.

70. D. Turnbull, Solid State Physics, 3 (1956), p.226.

71. J.C. Huang and A.J. Ardell, "On the Crystal Structure and Stability of T1 precipitates in Aged Al-Li-Cu Alloys", Department of Materials Science and Engineering, University of California, Los Angeles CA, Submitted to Materials Science & Technology (1986).

72. International Tables of X-ray Crystallography Vol.II

73. J.H. Kulwicki, T.H. Sanders Jr., Aluminum-Lithium Alloys II ed. T.H. Sanders Jr.and E.A Starke Jr., TMS-AIME, Warrendale PA, (1983) p.31.

74. W. Muller, "The Elastic Behavior of Al-Li alloys", Ph.D. Thesis, University of Stuttgart, 1985.

75. E. Kroner, Statistical Continuum Mechanics, Springer Berlin, 1971.

76. Aluminum: Properties and Physical Metallurgy, edited by J. E. Hatch, Metals Park, Ohio, ASM, (1984)

DISTRIBUTION LIST

Copy No.	
1 - 6	Director Naval Research Laboratory Washington, D.C. 20375 Attention: Code 2627
7	Dr. Bruce A. MacDonald, Manager Metallic Materials Program Code 1131M Office of Naval Research 800 North Quincy Street Arlington, VA 22217-5000
8 - 19	Defense Technical Information Center S47031 Building 5, Cameron Station Alexandria, VA 22314
20	W. W. Ruch, MS
21 - 22	E. A. Starke, Jr., MS
23	T. H. Courtney, MS
24 - 25	E. H. Pancake, Clark Hall
26	SEAS Publications Files
*	Office of Naval Research Resident Representative, N66002 Joseph Henry Building, Room 623 2100 Pennsylvania Avenue, N.W. Washington, D.C. 20037 Attention: Mr. Michael McCracken Administrative Contracting Officer

* send cover letter only

JO#9074:rsr

UNIVERSITY OF VIRGINIA
School of Engineering and Applied Science

The University of Virginia's School of Engineering and Applied Science has an undergraduate enrollment of approximately 1,500 students with a graduate enrollment of approximately 560. There are 150 faculty members, a majority of whom conduct research in addition to teaching.

Research is a vital part of the educational program and interests parallel academic specialties. These range from the classical engineering disciplines of Chemical, Civil, Electrical, and Mechanical and Aerospace to newer, more specialized fields of Biomedical Engineering, Systems Engineering, Materials Science, Nuclear Engineering and Engineering Physics, Applied Mathematics and Computer Science. Within these disciplines there are well equipped laboratories for conducting highly specialized research. All departments offer the doctorate; Biomedical and Materials Science grant only graduate degrees. In addition, courses in the humanities are offered within the School.

The University of Virginia (which includes approximately 2,000 faculty and a total of full-time student enrollment of about 16,400), also offers professional degrees under the schools of Architecture, Law, Medicine, Nursing, Commerce, Business Administration, and Education. In addition, the College of Arts and Sciences houses departments of Mathematics, Physics, Chemistry and others relevant to the engineering research program. The School of Engineering and Applied Science is an integral part of this University community which provides opportunities for interdisciplinary work in pursuit of the basic goals of education, research, and public service.

END

8-87

DTIC